



Norwegian University of  
Science and Technology

# Stress Concentrations and Stress Gradients at Elliptical Through-Holes and Spheroidal Cavities

**Kristine Klungerbo**

Master of Science in Mechanical Engineering

Submission date: August 2016

Supervisor: Gunnar Härkegård, IPM

Norwegian University of Science and Technology  
Department of Engineering Design and Materials



You can't expect God to entrust you with a big dream,  
if he can't trust you to make a small start.

- *Steven Furtick, Greater*



**MASTER THESIS SPRING 2016  
FOR  
STUD. TECHN. KRISTINE KLUNGERBO**

**Stress concentrations and stress gradients at elliptical through-holes and spheroidal cavities**

***Spenningskonsentrasjoner og spenningsgradienter ved elliptiske gjennomgående hull og sfæroidiske hulrom***

This assignment aims at a systematic and critical compilation of stress concentrations and stress gradients at elliptical through-holes and spheroidal cavities. The necessary data are based on available two- and three-dimensional analytical or numerical solutions from the open literature or on finite-element models developed in the framework of the present assignment. Wherever feasible, numerical (finite-element) solutions are to be compared with analytical predictions. In particular, analytical reference solutions are used to ensure sufficiently accurate finite-element modelling.

The compilation should cover a representative range of elliptical through-hole shapes and plate thicknesses. Spheroidal cavities with their axes parallel as well as perpendicular to the direction of loading are considered.

If time permits, it would be of interest to use the stress solutions together with criteria for fatigue at notches for assessment of the fatigue limit of members with elliptical through-holes or spheroidal cavities.

**Formal requirements:**

Three weeks after start of the thesis work, an A3 sheet illustrating the work is to be handed in. A template for this presentation is available on the IPM's web site under the menu "Masteroppgave" (<https://www.ntnu.no/web/ipm/masteroppgave-ved-ipm>). This sheet should be updated one week before the master's thesis is submitted.


Risk assessment of experimental activities shall always be performed. Experimental work defined in the problem description shall be planned and risk assessed up-front and within 3 weeks after receiving the problem text. Any specific experimental activities, which are not properly covered by the general risk assessment, shall be particularly assessed before performing the experimental work. Risk assessments should be signed by the supervisor and copies shall be included in the appendix of the thesis.

The thesis should include the signed problem text, and be written as a research report with summary both in English and Norwegian, conclusion, literature references, table of contents, etc. During preparation of the text, the candidate should make efforts to create a well-arranged and well-written report. To ease the evaluation of the thesis, it is important to

cross-reference text, tables and figures. For evaluation of the work, a thorough discussion of results is appreciated.

The thesis shall be submitted electronically via DAIM, NTNU's system for Digital Archiving and Submission of Master's theses.

The contact person at IPM for finite-element analyses is Bjørn Haugen.

  
Torgeir Welo  
Head of Division

  
Gunnar Härkegård  
Professor emeritus/Supervisor

 NTNU  
Norges teknisk-  
naturvitenskapelige universitet  
Institutt for produktutvikling  
og materialer

## Preface

This Master's Thesis is submitted for the *Master of Science degree in Mechanical Engineering*. The work is credited to The Department of Engineering Design and Materials at The Norwegian University of Science and Technology.

First of all, I want to acknowledge the great support from my supervisor, Professor Gunnar Härkegård. He has been the most important resource for me to reach as far as possible, and I could never have done this without him. Most of all, I want to thank him for being a wonderful person, for seeing me and understanding me. He has given me great motivation, and always seen my potential. I have learnt so much from working with him, and I am very grateful for this.

I would also like to thank my partner, Oddgeir Tveit, for the immense moral support throughout the writing of this thesis. I also need to thank him for being so wise, giving me great advice along the way.

Finally, for all my accomplishments in life, I owe my largest gratitude to my parents. Thank you for everything, I am forever thankful for all you have provided. May your strength live within me, always.



Kristine Klungerbo  
Trondheim, Norway  
July 2016





## Sammendrag

Effekten av tykkelse og Poissons tall på spenningskonsentrasjonen og spenningsgradienten ved roten av gjennomgående hull i plater er systematisk analysert ved hjelp av tredimensjonale elementanalyser. Effekten av Poissons tall på spenningskonsentrasjonen ved sfæroidiske hulrom og rundtgående spor i sylindre er også presentert ved hjelp av todimensjonale elementanalyser. Få løsninger eksisterer som tar høyde for effekten av den tredimensjonale materialoppførselen på spenningskonsentrasjonen. Denne masteroppgaven har som mål å utføre en systematisk gjennomgang av spenningskonsentrasjoner og spenningsgradienter for plater og sylindere. Formålet med dette er at de metodene og resultatene som presenteres kan benyttes for å utføre mer realistiske utmattingsberegninger.

Resultatene viser at spenningskonsentrasjonsfaktoren er sterkt påvirket av både Poissons tall og platetykkelsen.  $K_{t,max}$  befinner seg midt i platen for små tykkelser, men beveger seg ut mot den fri overflaten med økt tykkelse. For tykkere plater ligger  $K_{t,max}$  21.3% over  $K_{t,surf}$  for et sirkulært hull når  $\nu = 0.3$ , og forskjellen øker til 40% når  $\nu = 0.45$ . Resultatene viser også at spenningsgradienten har en tredimensjonal karakter. Ved hullranden av et sentralt gjennomgående hull er spenningsgradienten lavest der  $K_t = K_{t,max}$  og høyest ved den fri overflaten. Verdien av den laveste spenningsgradienten ligger 1% under den analytiske verdien. Noe som betyr at den laveste spenningsgradienten befinner seg i det samme punktet som den maksimale spenningen, og materialvolumet i dette området er derfor under mye høyere belastning enn hva konvensjonelle metoder for utmatting tar høyde for. Utmattingsberegninger basert på resultatene fra elementanalysene viser at levetiden man finner ved konvensjonelle metoder er mye høyere enn i virkeligheten. Hvis analytiske løsninger anvendes for å beregne levetiden til en plate, kan dette medføre en levetid som er 57.7%, høyere enn ved bruk av tredimensjonale numeriske resultater. Dette skaper bekymringer for dagens metoder og understreker viktigheten av forskning på dette området.



## Abstract

The effect of thickness and Poisson's ratio on the stress concentration factor and the stress gradient at the notch root of central elliptical through-holes in plates are systematically investigated using three-dimensional finite element method. The effect of Poisson's ratio on the stress concentration factor at central spheres and circumferential grooves in cylinders is also presented using two-dimensional finite element method. Few solutions in literature considers the three-dimensional behaviour of structures, even though it greatly affects the properties of the stress concentration factor. This research aims to provide a systematic and critical presentation of the stress concentration factors and stress gradients for plates and cylinders. Ultimately, the goal is to provide methods and data that allows for more reliable fatigue assessments.

The results show that the stress concentration factor is strongly dependent on the shape of the irregularity, the plate thickness and the Poisson's ratio. It is found that  $K_{t,max}$  moves from the mid-plane towards the free surface of the plate with increasing thickness, but never reaches it. For large thicknesses,  $K_{t,max}$  is 21.3% higher than  $K_{t,surf}$  for a circular hole when  $\nu = 0.3$ , and the difference increases to 40% when  $\nu = 0.45$ . The stress gradient at the notch root of a central through-hole is lowest where  $K_t = K_{t,max}$  and highest at the free surface of the plate. The value of the lowest stress gradient lies 1% below the analytical value. With the lowest stress gradient positioned at the point of maximum stress, the volume of highly stressed material is larger than accounted for by conventional methods for fatigue calculations. A fatigue assessment based on the finite element results show that the fatigue life is drastically overestimated by conventional methods. An analytical approach leads to an overestimated fatigue life of 57.7%, compared to a calculation based on the three-dimensional numerical results. This rises concerns about the conventional methods, and highlights the importance of research within this field.



# Contents

Preface	v
Sammendrag	vii
Abstract	ix
<b>1 Introduction</b>	<b>1</b>
<b>2 2D FEA as a preliminary reliability study</b>	<b>3</b>
2.1 Stress concentration at central holes in plates . . . . .	3
2.1.1 Circular holes . . . . .	3
2.1.2 Elliptic holes . . . . .	6
2.1.3 Holes with U-shaped ends . . . . .	7
2.1.4 Conclusion on mesh requirements based on 2D FE results . .	10
2.2 Stress gradients at central holes in plates . . . . .	14
2.2.1 Analytical solution . . . . .	14
2.2.2 Effect of nodal averaging on the FE-results . . . . .	14
2.2.3 Finding the correct stress gradient from the FE-results . . .	16
2.3 Stress concentration at side-grooves in plates . . . . .	20
2.3.1 Semicircular side-grooves . . . . .	21
2.3.2 Semi-elliptic side-grooves . . . . .	21
2.3.3 U-shaped side-grooves . . . . .	22
<b>3 2D FEA used for 3D evaluation of structures</b>	<b>23</b>
3.1 Theoretical approach to plane strain . . . . .	23
3.1.1 Hooke's law . . . . .	23
3.1.2 Plane strain . . . . .	25
3.1.3 Generalised plane strain . . . . .	25
3.2 2D FEA of plates in plane strain . . . . .	26
3.2.1 Central circular holes . . . . .	27
3.2.2 Semicircular side-grooves . . . . .	27
3.3 3D cylinders from 2D axisymmetric FE-models . . . . .	30
3.3.1 Central spheres and spheroids . . . . .	30
3.3.2 Circumferential grooves . . . . .	33
3.4 Similarities between cylinders and plates in GPE . . . . .	36
<b>4 3D FEA of plates with central holes</b>	<b>39</b>
4.1 3D modelling technique . . . . .	39
4.2 Plane strain solution . . . . .	41
4.3 The 3D stress distribution . . . . .	42

4.4	The effect of thickness . . . . .	46
4.4.1	The effect of thickness on the stress concentration factor . .	46
4.4.2	The effect of thickness on the transverse stress . . . . .	51
4.4.3	The effect of thickness on the stress gradient . . . . .	53
4.5	The effect of Poisson's ratio . . . . .	57
4.5.1	The effect of Poisson's ratio on the stress concentration factor	57
4.5.2	The effect of Poisson's ratio on the transverse stress . . . . .	60
4.5.3	The effect of Poisson's ratio on the stress gradient . . . . .	60
<b>5</b>	<b>Fatigue assessment based on 3D FEA</b>	<b>65</b>
5.1	Formulae for fatigue . . . . .	65
5.1.1	The peak stress method . . . . .	65
5.1.2	The gradient method . . . . .	66
5.2	Fatigue constants . . . . .	67
5.3	Fatigue life calculations . . . . .	67
5.3.1	The peak stress method . . . . .	67
5.3.2	The gradient method . . . . .	68
5.4	Conclusion on fatigue life . . . . .	69
<b>6</b>	<b>Discussion of method</b>	<b>71</b>
<b>7</b>	<b>Conclusion</b>	<b>73</b>
7.1	Key findings . . . . .	73
7.2	Further work . . . . .	74
	<b>Bibliography</b>	<b>75</b>
<b>A</b>	<b>Appendix: The finite element models</b>	<b>77</b>
A.1	Input parameters for the FE-model . . . . .	77
A.2	The 3D structures studied . . . . .	77
A.3	Boundary conditions for FEA . . . . .	79

## List of Figures

1	The geometry of 2D plates with central holes . . . . .	4
2	$K_t$ from FEA for a thin plate with a central circular hole . . . . .	5
3	$K_t$ from FEA for a thin plate with a central elliptic hole . . . . .	7
4	Geometry of a hole with U-shaped ends . . . . .	8
5	Results from FEA for holes with U-shaped ends . . . . .	9
6	$K_t$ when element size $h$ goes towards zero . . . . .	13
7	Accuracy of $K_t$ with changing $h/\rho$ of smallest element . . . . .	13
8	The 2D mesh closest to the notch . . . . .	15
9	Two different approaches to find $K_t$ from FEA . . . . .	17
10	Stress gradients for 2D plates with a central circular hole . . . . .	18
11	The stress gradient solution for varying $h/\rho$ . . . . .	19
12	The stress gradient solution for varying $a/w$ . . . . .	19
13	The different coordinate systems for plates and cylinders . . . . .	24
14	SCF results for plates with central holes in PE and GPE . . . . .	28
15	SCF results for plates with side-grooves in PE and GPE . . . . .	29
16	SCF results for a cylinder with a central sphere . . . . .	32
17	Stress gradient for a cylinder with a central sphere . . . . .	32
18	SCF results for a cylinder with circumferential grooves . . . . .	35
19	Stress gradient for cylinder with circumferential grooves . . . . .	35
20	Comparing the transverse SCF in cylinders and plates . . . . .	37
21	3D FE-mesh for a plate with a central circular hole . . . . .	40
22	Results from 3D FEA with full and reduced integration . . . . .	43
23	Typical 2D stress distribution ahead of notches . . . . .	44
24	Contour plots of the 3D stress distribution ahead of a notch . . . . .	45
25	Change in maximum SCF with increasing plate thickness . . . . .	46
26	SCF through the thickness of plates . . . . .	48
27	Location of $K_{t,max}$ inside the plate . . . . .	50
28	Maximum SCF compared to the value at the free surface . . . . .	50
29	Change in transverse SCF through the thickness . . . . .	52
30	Stress gradient distribution through the thickness . . . . .	54
31	The variation of $\chi\rho$ with increasing thickness . . . . .	56
32	$K_{t,max}$ for circular holes with varying thickness and Poisson's ratio .	58
33	$K_{t,max}/K_{t,surf}$ for varying Poisson's ratio . . . . .	59
34	$K_{tz,max}$ for circular holes with varying thickness and Poisson's ratio	61
35	The stress gradient for varying Poisson's ratio . . . . .	63

## List of Tables

1	$K_t$ from FEA for a central U-shaped hole . . . . .	9
2	FE-results for spheroidal cavities in cylinders . . . . .	33
3	FE-results for circumferential grooves in cylinders . . . . .	34
4	$K_t$ from 2D FEA and 3D FEA to compare accuracy . . . . .	42
5	Constants used for fatigue calculations . . . . .	67
6	Fatigue life by the peak stress method . . . . .	67
7	Fatigue life by the gradient method . . . . .	68



# Nomenclature

$\chi$	Relative stress gradient
$\nu$	The Poisson's ratio
$\rho$	Radius of curvature at the notch root of the ellipse
$\sigma_x$	Local stress in $x$ -direction at notch root
$\sigma_y$	Local stress in $y$ -direction at notch root
$\sigma_z$	Local stress in $z$ -direction at notch root
$\varepsilon_\phi$	Strain in the circumferential direction of cylinders
$\varepsilon_z$	Strain through the thickness of plates
$a$	Horizontal (major) radius of the ellipse
$b$	Vertical (minor) radius of the ellipse
$h$	Length of the element at the notch-root
$K_{t,\max}$	The through-thickness maximum stress concentration factor
$K_{t,\text{surf}}$	The stress concentration factor at the free surface of the plate
$K_t$	The gross stress concentration factor
$K_{t\infty}$	Analytical stress concentration factor
$S$	Remotely applied stress
$t$	Half-thickness of plate
$w$	Half-width of plates and cylinders
$z_{\max}$	The position of maximum SCF through the thickness
FEA	Finite element analysis
FEM	Finite element method
GPE	Generalised plane strain
PE	Plane strain
PS	Plane stress
SCF	Stress concentration factor



# 1 Introduction

Structural irregularities, such as holes and grooves, cause a local stress concentration that exceeds the applied load. The magnitude of such, depends on the shape of the irregularity, but challenges the fatigue life of the structure. For brevity, the term notch will be used in reference to any structural irregularity.

The local stress concentration caused by the notch is highest at the notch root, and measured by the stress concentration factor (SCF). The SCF is labelled  $K_t$  and calculated from

$$K_t = \frac{\sigma_{\max}}{S} \quad (1)$$

where  $\sigma_{\max}$  is the maximum stress at the notch root, and  $S$  is the applied stress. As this thesis only considers the gross SCF, the expression  $K_t$  is sufficient.

Some of the first classical solutions for SCFs in infinite plates were developed by Kirsch [1], Kolosov and Inglis [2]. These are, to this day, valuable analytical solutions. For central spheres in cylinders, some analytical solutions are developed by Neuber [3], Timoshenko and Goodier [2], and Barber [4]. Many solutions considering the finite width also exist [5], [6]. Engineering handbooks such as Peterson [6] present solutions for a wide variety of problems, and is a valuable tool for engineers. Most of the SCFs presented in engineering handbooks are based on analytical and numerical solutions for thin plates, and there are no readily available solutions that consider the three-dimensional properties of structures.

The great improvements of computers has made it possible to perform three-dimensional finite element analyses (FEA) of high accuracy. Some recent papers have considered the three-dimensional effects on SCF with the help of FEA. The results by She and Guo [7] show that the maximum SCF varies with increasing thickness, and that the value always lies above both the analytical solution and the value found at the free surface. Yu et al. [8] shows that the SCF also increases significantly with Poisson's ratio, for all plate thicknesses. Vaz et al. [9] studied the finite-width effect, and found that the SCF-response to changes in thickness also depends on the plate width. If the three-dimensional effect on the SCF gives results that exceed the analytical solution, this makes fatigue calculations unreliable. Bellet et. al. [10] studied the fatigue behaviour of 3D SCFs and showed that the commonly used 2D solutions for the notch fatigue assessment results in false prediction of fatigue life.

The relative stress gradient was introduced by Siebel and Stieler [11], and the table with relative stress gradients that was presented then, is practically the only one that is widely known [12]. In a recent article, Filippini [12] compared the accuracy of different stress gradients, calculated from various analytical and numerical stress solutions. He found that it was difficult to correctly capture the

gradient based on the solutions that he considered. No approaches to estimate the stress gradient in literature involve considering the three-dimensional effects, or even using results from FEA to calculate the stress gradient. This means that the three-dimensional behaviour of the stress gradient is unknown.

The purpose of this thesis is to provide a systematic and critical presentation of three-dimensional SCFs and stress gradients, in an attempt to make fatigue assessments more reliable. The thesis begins with a preliminary study that aims to prove that FEA is a powerful tool to estimate stress concentration factors and stress gradients, for both plates and cylinders with irregularities. The preliminary study is based on 2D FEA and the FE-results are compared to known analytical solutions.

In the second part, an approach to evaluate 3D behaviour based on results from 2D FEA is presented. The results from 2D FEA of plates in plane strain and generalised plane strain are presented, and then these results are compared to the results from 2D axisymmetric FEA of cylinders. The third part of the thesis contains the main study of 3D FEA, where the focus is on plates with central holes. Here the effect of notch shape, thickness and Poisson's ratio on the SCF and the stress gradient is carefully evaluated. In the fourth part, to demonstrate the importance of the results from 3D FEA, a fatigue assessment is performed, based on the data collected from FEA. Finally, an appendix that contains figures and information about all the FE-models used, is provided at the end.

In the description of the master thesis there is one topic that is mentioned that will not be included. This is the spheroidal cavities with their axis perpendicular to the direction of loading, as it was decided that focusing solely on 3D plates would be more valuable.

## 2 2D FEA as a preliminary reliability study

For finite element (FE) modelling of notches in thin plates, a 2D model subjected to plane stress is a common approach, where the plane stress condition is used to replicate the correct behaviour of thin plates. The numerical accuracy can be tested by comparing the FE results to analytical solutions that are available for some geometries. From this, the desired accuracy for a 2D model can be reached through mesh refinement.

Additionally, the preliminary study of 2D models is an important benchmark for reliable 3D finite element analysis (FEA), as few solutions considering the thickness of plates exist and no analytical 3D solutions are available.

### 2.1 Stress concentration at central holes in plates

#### 2.1.1 Circular holes

The first analytical solution to stress concentrations was found by Kirsch [2] in 1898, when he described the stress field around a circular hole in an infinitely wide plate as shown in Figure 1a. Kirsch's solution for a plate with a circular hole is found in *Theory of Elasticity* [2] and may be expressed in the following way:

$$K_t = \frac{(\sigma_y)_{y=0}}{S} = 1 + \frac{1}{2}\left(\frac{a}{x}\right)^2 + \frac{3}{2}\left(\frac{a}{x}\right)^4 \quad (2)$$

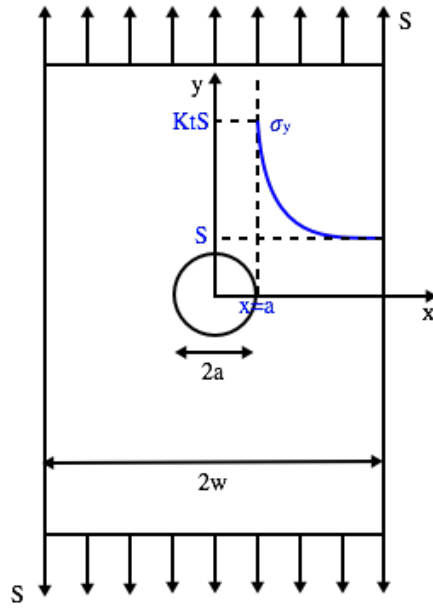
where  $\sigma_y$  is the local stress in the  $y$ -direction at  $x = a$ ,  $S$  is the nominal stress at the gross section, and  $a$  is the radius of the hole.

As the stress concentration factor (SCF) is largest at the notch root [2], this is the region of interest, see Figure 1a. The analytical solution at the notch root of a circular hole in an infinite plate, where  $x = a$ , is:

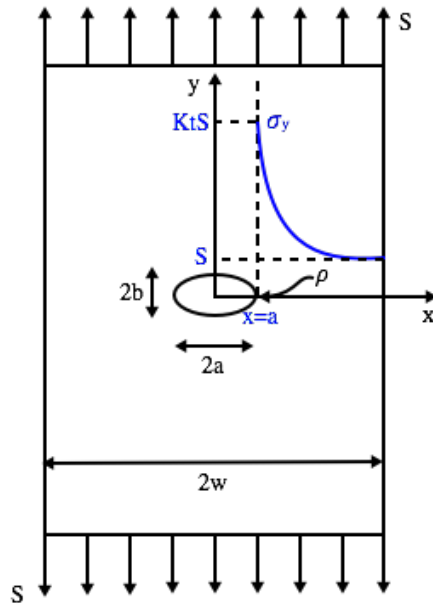
$$K_{t,\infty}(x = a) = 1 + \frac{1}{2} + \frac{3}{2} = 3$$

where the subscript  $\infty$  is used to emphasise that this is the analytical solution for an infinite plate, a value that will be used later to evaluate the accuracy of the FE results.

With finite element method (FEM) a high local accuracy can be applied to the region of interest, saving computation time on the other regions. Because of this, the mesh is finest close to the notch root, with an increasing element density towards the notch root in order to accommodate for the high stresses in this region. For best accuracy, the element at the notch root should have straight perpendicular edges of equal length because the square is the most natural shape of the element [13]. The element at the notch root is also the smallest element in the mesh, with a non-dimensional element size  $h/\rho$ , where  $h$  is the length of the



(a) Kirsch's circular hole



(b) Inglis' elliptic hole

Figure 1: The geometry of 2D plates with central holes, as studied by Kirsch for circular holes and Inglis for elliptic holes (if  $w = \infty$ ). See Eq. (2) and (4).

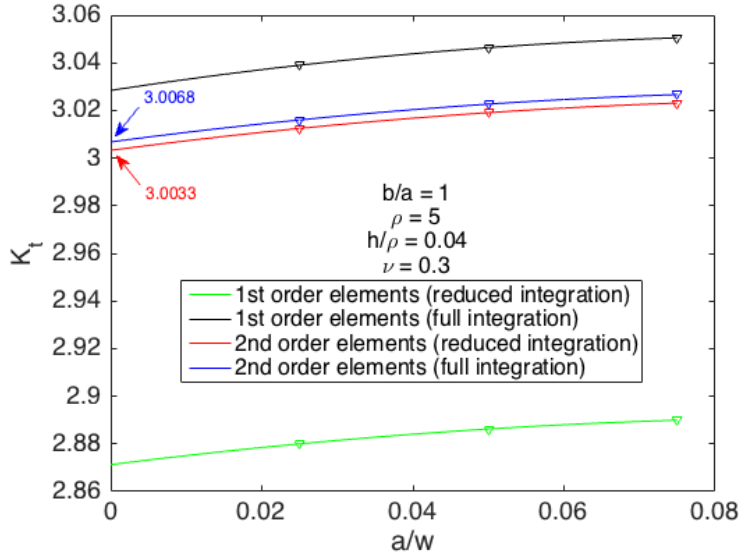


Figure 2:  $K_t$  from FEA for a thin plate with a central circular hole for varying  $a/w$ . The results with full and reduced integration, as well as 1st and 2nd order elements are presented.

edges (it is a square, so all sides are equal) and  $\rho$  is the radius of curvature at the notch root. It is expected that the accuracy increases with more elements [13], but is not automatically achieved, and the effect of  $h/\rho$  on FEA and what values to choose for further analyses will be investigated in a later section.

With a fine mesh close to the notch root and a square element at the notch root, the results from FEA should be close to the analytical solution. Figure 2 shows the results from a 2D FEA of a plate with a central circular hole where  $h/\rho = 0.04$ . The hole-radius to plate-width ratio  $a/w$  was varied between 0.025 and 0.075 to allow for an extrapolation to  $a/w = 0$ . As  $a/w = 0$  the plate width is infinite and can be compared with the analytical solution. From Figure 2 it is evident that  $K_t$  gets closer to the analytical solution when  $a/w$  decreases. The best FEA result gives  $K_t = 3.0033$ , which is a deviation of 0.11% from the analytical solution, showing that it is possible to use FEA to determine SCF-values in good correspondence with analytical solutions.

Four different graphs are plotted in Figure 2, showing the effect of four different settings that can be chosen for FE calculations. Firstly, a choice between first order elements and second order elements must be made, which in practice is a choice of how many nodes the element has (four or eighth), but mathematically it is the choice of polynomial to describe the element, either linear or quadratic. Secondly, a choice between full and reduced integration is presented, which in practice is a

choice between trying to calculate the results by the lowest over-estimate or by the lowest under-estimate. Combinations of these four parameters give the following four element properties: 1F, 1R, 2F and 2R, which is what they are called from this point, for brevity. Plots for several notch shapes will be studied before deciding which of these parameters to use further, but already in Figure 2 the 1F element shows a large error compared to the other FE results and the analytical solution. The difference between 2F and 2R however, is very small.

### 2.1.2 Elliptic holes

Research on the stress distribution ahead of notches continued, and in 1909 and 1913, Kolosov and Inglis [1] developed analytical solutions for the stress concentration near elliptic holes in infinite plates. Schijve presents the result in *Fatigue of Structures and Materials* [14], where the analytical equation is written as follows:

$$K_t = \frac{(\sigma_y)_{y=0}}{S} = 1 + \frac{a(a-2b)(x-\sqrt{x^2-c^2})(x^2-c^2) + ab^2(a-b)x}{(a-b)^2(x^2-c^2)\sqrt{x^2-c^2}} \quad (3)$$

where  $a$  is the semi-major axis of the ellipse and  $b$  is the semi-minor axis, as shown in Figure 1b, and  $c = \sqrt{a^2 - b^2}$ .

With the use of Eq. (3),  $K_t$  for any elliptical through-hole in an infinite plate can be found. The stress concentration is highest at the notch root, where  $x = a$ , and inserting this into Eq. (3) gives

$$K_t(x = a) = 1 + 2 \left( \frac{a}{b} \right) \quad (4)$$

which is a well-known function that applies for any elliptic shape in 2D plates of infinite width, including circular holes.

Eq. (4) shows that the SCF increased when the ellipse flattens. The radius of curvature  $\rho$  at the notch root of an ellipse is given by  $\rho = b^2/a$ , see Figure 1b, so that the SCF increases with decreasing radius of curvature at the notch root. As an example, if  $b = 0.5a$  and  $\rho = 1.25$ , Eq. (4) gives

$$K_t(x = a) = 1 + 2 \left( \frac{1}{0.5} \right) = 5$$

showing that the SCF is significantly higher than for a circular hole and hence increases with decreasing radius of curvature. It is evident that the stress gradient at the notch root increases accordingly.

As long as  $b < a$ , the stresses ahead of elliptical holes are higher than for circular holes and a finer mesh is required to capture this accurately. The actual dependence between element size and curvature  $h/\rho$  is studied closely in Section 2.1.4,



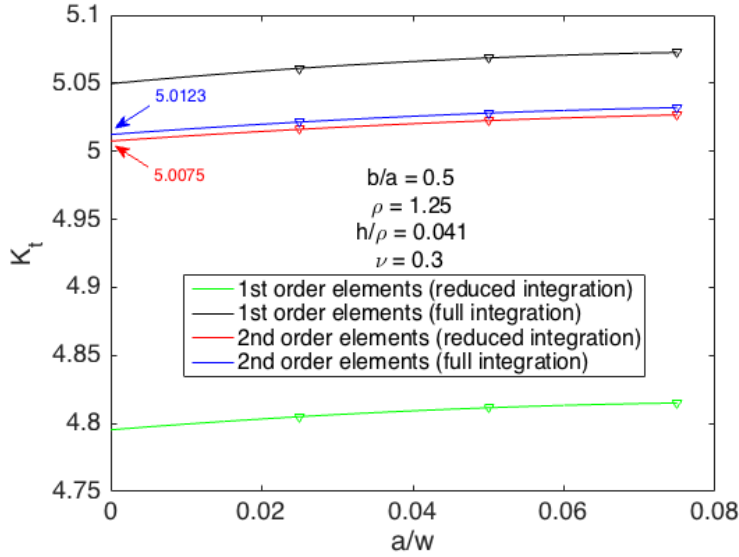


Figure 3:  $K_t$  from FEA for a thin plate with a central elliptic hole for varying  $a/w$ . The results with full and reduced integration, as well as 1st and 2nd order elements are presented.

but the number of elements in the FE model can quickly be increased and shifted closer to the notch root, to increase the element density in the region of interest. The FE results with  $h/\rho = 0.041$  for 2D plates with central elliptic holes where  $\rho = 1.25$  and for varying  $a/w$  is presented in Figure 3.

The FE results for an ellipse, when extrapolated to  $a/w = 0$ , gives  $K_t = 5.0075$  as the closest result to the analytical solution from Eq. (4). The FEA solution only deviates 0.15% from the analytical solution, again confirming that FEA is a satisfyingly accurate tool. Figure 3 shows the results from using all the element settings, both 1st and 2nd order elements with full and reduced integration, just like in Figure 2. Again, it is observed that the first order elements are further away from the analytical solution than the second order elements, and that the 1R elements are most inaccurate.

### 2.1.3 Holes with U-shaped ends

With the equation for the stress field around central elliptical holes, a wide variety of notches were covered, but the remaining question was whether this description could have any relation to notches with similar - but not elliptic - shapes. Inglis found out that the stress concentration factor at the notch root of a central through-thickness irregularity in an infinite plate was almost solely dependent on the semi-major axis  $a$  and the elliptical shape at the notch root [1]. If the notch

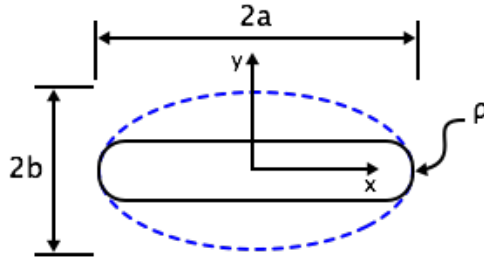


Figure 4: Hole with U-shaped ends, where the ends merge smoothly into an ellipse.

root of an irregularity is approximately elliptic in shape, Inglis suggested that the SCF could be found by replacing the irregularity with an ellipse with the same semi-major axis  $a$  and radius of curvature  $\rho$ , see Figure 4.

Inglis continued by showing that, if this was true, inserting the radius of curvature  $\rho = b^2/a$  into Eq. (4) would be practical. The equation takes the following form

$$K_t(x = a) = 1 + 2\sqrt{\frac{a}{\rho}} \quad (5)$$

where the radius of curvature at the notch root of any central notch with similar geometry to an ellipse can be inserted.

A hole with U-shaped ends is classified as being similar to an ellipse if it has the same radius of curvature at the notch root [6], this because it then merges smoothly into an ellipse at the notch root, see Figure 4. If this criteria is satisfied, Eq. (5) should give a good approximation of the SCF for central holes with U-shaped ends. As an example, if the U-notch has a radius of curvature  $\rho = 1.25$ , the analytical solution is  $K_t = 5$  and the results from FEA are expected to come close to this value. Figure 5 shows the  $K_t$  results from FEA for varying  $a/w$ , where by an extrapolation to  $a/w = 0$  a deviation of 2.27% and 2.17% for full and reduced integration respectively. In Figure 5 only 2F and 2R elements are studied, as the solutions for first order elements fell outside of the figure, again because they showed low accuracy compared to second order elements. A final evaluation of the different mesh parameters will be carried out in the next section.

The SCF found through FEA gives a significant error relative to Eq. (5), but in this case it is not because the results are inaccurate. In fact, Peterson [6] found that the result for holes with U-shaped ends might be up to 2% higher than the value for an elliptical hole with the same curvature at the notch root. Comparing the FE result for the U-shaped hole and the ellipse it is found that  $K_t$  for a U-shaped

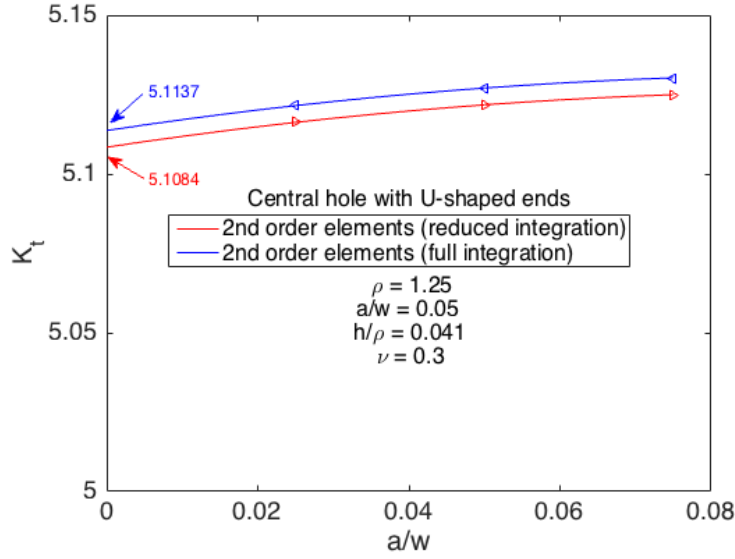


Figure 5:  $K_t$  for plates with central holes with U-shaped ends for varying  $a/w$ .

Table 1:  $K_t$  from FEA for a central U-shaped hole and a central ellipse, where both models have  $a/w = 0.05$ ,  $\rho = 1.25$  and  $h/\rho = 0.041$ .

	$K_t$ FEA
U-shape	5.12604
Ellipse	5.029468

hole is 1.92% higher than for the ellipse when both have a radius of curvature  $\rho = 1.25$ , see Table 1. The U-shaped hole cause higher stress concentrations than an elliptic holes because the ellipse changes in shape continuously, ensuring that stresses gradually redistribute around the hole. The U-shaped hole however, cause abrupt changes in the stress distribution around the hole, resulting in higher stresses at the notch root. The radius of curvature at the notch root helps to better redistribute the stress, explaining why the solutions for  $K_t$  may still be within 2% of each other.

The properties of a U-shaped hole - relative to a circle and an ellipse - gives a wide understanding of how any central notch affects the stress distribution, and the effect of different shape parameters. As the results are conclusive, the central hole with U-shaped ends will not be investigated further in this thesis, also because it is assumed that the deviation from the elliptical results will be of a similar size for 3D structures.

#### 2.1.4 Conclusion on mesh requirements based on 2D FE results

By increasing the number of elements in the mesh, the accuracy of the FEA solution improves, but the computation time increases accordingly [15]. With a preliminary study, the mesh performance can be carefully evaluated to assure the highest accuracy possible at reasonable computational cost.

##### Choosing a value $a/w$ for FE modelling:

As it would be inefficient to model an infinite plate, Figures 2, 3 and 5 can be used to determine a ratio  $a/w$  that seems reasonable for FEA. A region at which  $K_t$  is barely affected by the finite width of the plate is desirable, as the actual effect that  $a/w$  has on  $K_t$  is not fully understood. The desired  $a/w$  gives an SCF that lies within a small deviation from the analytical solution, but the choice has to be a compromise between the smallest deviation and the fact that  $a/w$  should be of a realistic real-life size.

From Figures 2 and 3 the SCF decreases towards the analytical solution with decreasing  $a/w$ , as would be expected. Ideally, to make the best choice for  $a/w$ , plates with several  $a/w$  ratios would be modelled in 3D, but this is not possible due to computation time. Because of this, the decision is made based on the 2D results. The value  $a/w = 0.05$  is chosen because the finite-width effect is minimal and the size is also practical for modelling. An important reason for this choice is that in the papers by She and Guo [7] and Yu et al. [8] the same value for  $a/w$  was used, so it makes it very practical for comparing results. Vaz et al. [9] studied the effect of the finite width and concluded that when  $a/w \leq 0.05$  the SCF results were basically unaffected by plate width.

##### Choosing first or second order elements:

From FEM theory, elements allowing curved edges were expected to show best results along the edge of the hole [15], due to the curvature. The elements allowing curved edges are described by quadratic polynomials rather than linear polynomials, which would give a better approximation of a curved boundary. The choice between these properties in FEA is made when applying first or second order elements, where the first order elements are those described by linear polynomials and the second order elements are those described by quadratic polynomials [13].

In practice, what is decided is how many nodes that will be used in the calculation of each element. If a rectangular 2D element is used as an example, first order elements only uses nodes at each of the corners, while second order elements use an additional node at every edge of the element. This leads to four nodes in a first order element and eight nodes in a second order element, which for a 3D element - using the same example - would give eight and twenty nodes respectively.

As 2D FEA is a relatively quick procedure, it was possible to test both first and second order elements during the preliminary study, to compare the behaviour, as shown in Figures 2 and 3. The SCF results are very consistent, however the second order elements outperform the first order elements in all cases that are studied. In Figure 5, the solutions with first order elements even ended up outside the figure. For the second order elements, the solutions at  $a/w = 0$  are satisfyingly close to the analytical solutions, and based on all the preliminary results, using second order elements is the obvious choice as it provides much higher accuracy.

The computation time is the only factor that could possibly force the need for first order elements in 3D FEA, but when the difference in accuracy is as large as the preliminary study shows, second order elements are needed for reliable results regardless of the increase in computation time.

### **Choosing full or reduced integration:**

After deciding how many nodes each element should have, the numerical integration method used to calculate the stiffness matrix for each element must be chosen.

The nodal forces for one element are directly related to the nodal displacements via the element stiffness matrix [13]. This is the local stiffness matrix that controls the coupling between all forces and displacements at all nodes in the element. The global stiffness matrix couples every local stiffness matrix with the global forces and displacements. Each element of the global stiffness matrix is an integral that is calculated by numerical integration [13].

For numerical integration, FEM applies an integration formula called Gauss quadrature to integrate the element polynomials as exactly as possible. The special property of the Gauss quadrature is that the first term integrates a 1st order polynomial exactly, the second term integrates a 3rd order polynomial exactly and the third term integrates a 5th order polynomial exactly. Full integration chooses the lowest number of terms from the Gauss quadrature that are needed to exactly integrate the stiffness matrix, which often results in an over-integration because the element stiffness matrix often has 2nd or 4th order polynomials [13]. Reduced integration chooses the term that is one lower than for full integration, sometimes ending up with a more accurate solution [13].

As both integration methods have some weaknesses, a comparison was given in Figures 2, 3 and 5. All figures show the same consistent behaviour, where full integration lies slightly above reduced integration for all  $a/w$ . In fact, the accuracy of both methods is satisfying compared to the analytical solution at  $a/w = 0$ . As reduced integration lies closer to the analytical solution it seems to be the best choice, but both methods have some weaknesses in 3D [13]. Thus it is safest to control the accuracy by 3D FEA, and the results are presented in a later section.

### Choosing a satisfying value $h/\rho$ for FE mesh:

By comparing Figures 2 and 3 it shows that an ellipse with  $b/a = 0.5$  requires a finer mesh in order to reach the same accuracy as for a circular hole. This accelerated an investigation of the link between the radius of curvature  $\rho$  at the notch root and the length  $h$  of the smallest element at the notch root. The investigation involved up to eight different 2D FEAs with refined meshing at the notch root, and was performed for both plates with elliptical and circular holes. To assure that all analyses were as reliable, the perfectly square shape of the notch-root element was maintained, even though the size was varied.

As no analytical solutions for finite-width plates with central holes exists, rather than following other available numerical approaches, a new approach was introduced. The new approach was based on the idea that if the element density increases drastically, the size of the smallest element goes towards zero. Because the accuracy of a FE model increases with increasing number of elements [13], perfect accuracy should be achieved when  $h = 0$ . Figure 6 shows the differences in  $K_t$  that was found for varying  $h$ , and the polynomial that was used and extrapolated to  $h = 0$ . This is a numerical approach to determine the assumed accurate solution,  $K_{t,h=0}$ . The scaling at the  $y$ -axis in Figure 6 was chosen for practical reasons, so that both graphs could be shown in the same figure as the important result is the value of the polynomial at  $h = 0$ .

In Figure 7 the  $K_t$  results from FEA for both the ellipse and the circle are normalised by the suggested numerical solution. The results are plotted for varying  $h/\rho$  values, and the graphs for an ellipse and a circle coincide. This means that the same accuracy is found in a plate with a central elliptic hole and a central circular hole, as long as the same  $h/\rho$  value is used. The analysis presented in Figure 7 was calculated with 2F elements, but almost exactly the same results are found with 2R elements due to the normalisation of the  $y$ -axis.

Figure 7 is an important resource, as it gives the expected accuracy of an FE model for any given  $h/\rho$ , and the results are actually specific for  $a/w = 0.05$ . It is found from the figure that for  $h/\rho \geq 0.06$  the solutions for the ellipse and circle begin to separate. This is not surprising, as both solutions are becoming less accurate with increasing  $h/\rho$ , and the two different notch types will naturally cause different behaviour under inaccurate conditions.

When choosing a  $h/\rho$  value to use for further analyses, it is most important to consider the computation time involved for the elliptic hole, as it requires a much finer mesh. Trial and error with 3D FEA was used to find a satisfying value that the computer could solve, and  $h/\rho = 0.06$  was chosen. With this value, the expected error is 0.1%, which is extremely low. An accuracy of this level is not needed for fatigue life calculations, as errors up to 1% will have minor effects on the fatigue life, but results of high accuracy are always desired.

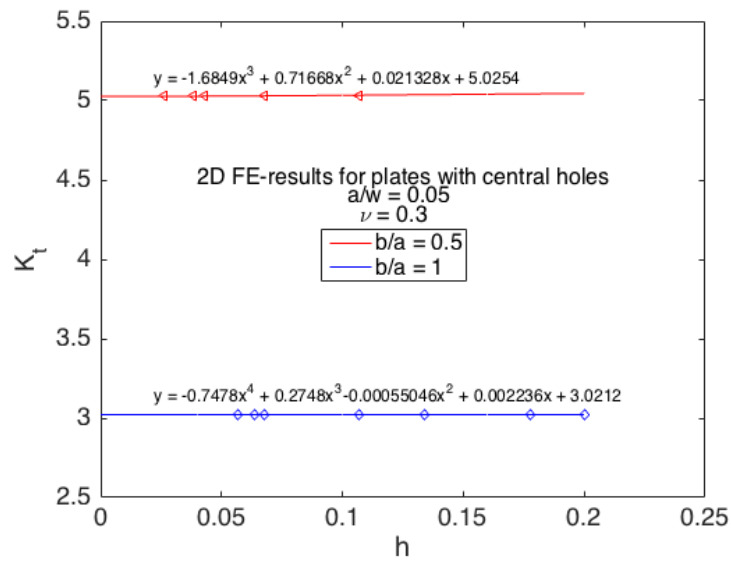


Figure 6: The values of  $K_t$  as the element size  $h$  goes towards zero.

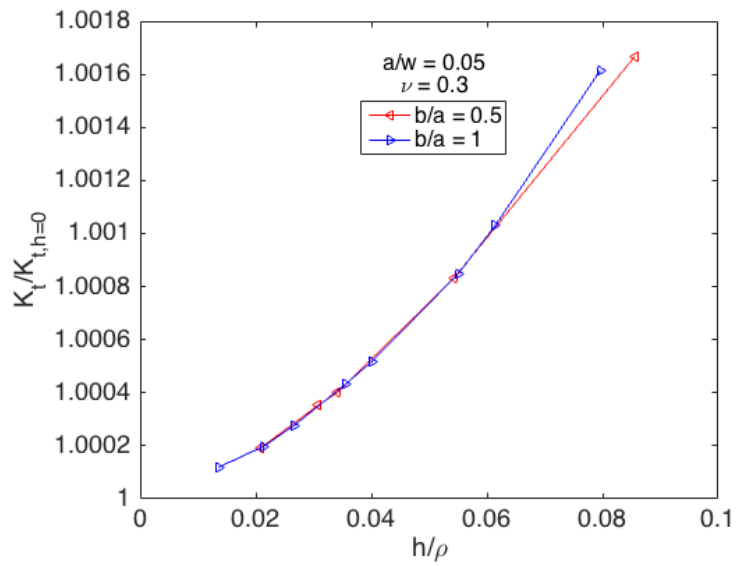


Figure 7: Accuracy of  $K_t$  with changing element size  $h/\rho$  at the notch root.

## 2.2 Stress gradients at central holes in plates

Both the analytical solutions and the results from finite element analysis show that the maximum stress at the notch root is much higher than the remotely applied stress. Such high stress concentrations cause high stress gradients, which affect fatigue assessment [16]. Estimating the stress gradient based on the results from FEA allows for a quick and specific fatigue assessment, as will be shown in section 5. The stress gradient is simply the rate of change in stresses at the notch root, but it is not as straight forward to correctly calculate this value from FEA. The resulting gradient depends on the number of nodes considered in the calculation and the accuracy of the FE model.

### 2.2.1 Analytical solution

The value of the stress gradient changes with the radius of curvature at the notch root, and the term «relative stress gradient» is commonly used. The relation between the relative stress gradient  $\chi$  and the local stress  $\sigma_y$  was defined by Siebel and Stieler [11], and is given by

$$\chi = \left| \frac{\{d\sigma_y(x)/dx\}_{x=a}}{\sigma_y(x=a)} \right| \quad (6)$$

where  $\sigma_y$  is the stress function in terms of the distance  $x$  away from the notch root, while  $\sigma_y(x=a)$  is the maximum stress at the notch root [14].

However, it is most natural to express the gradient together with the radius of curvature  $\rho$ , and the product  $\chi\rho$  is introduced. In the following, this product is what will be referred to as the «stress gradient». Schijve [14] showed that the stress gradient for an elliptic trough-hole in an infinite plate could be calculated from Eq.(6) by inserting Eq.(3), which gives

$$\chi\rho = \left(2 + \frac{1}{K_t}\right)$$

so that for a circular hole where  $K_t = 3$ , the stress gradient  $\chi\rho = 7/3$ .

### 2.2.2 Effect of nodal averaging on the FE-results

To determine the stress gradient from FEA, all the data about the stress field close to the notch root is needed. It requires a lot of time, for 3D FEA in particular, to extract all this data from the results. In the process of collecting large amounts of data from many FE models, the quickest way is to collect data from the corner nodes of each element, nodes 1-4 in Figure 8a. However, these values are not theoretically accurate. The stresses are most accurately calculated at the



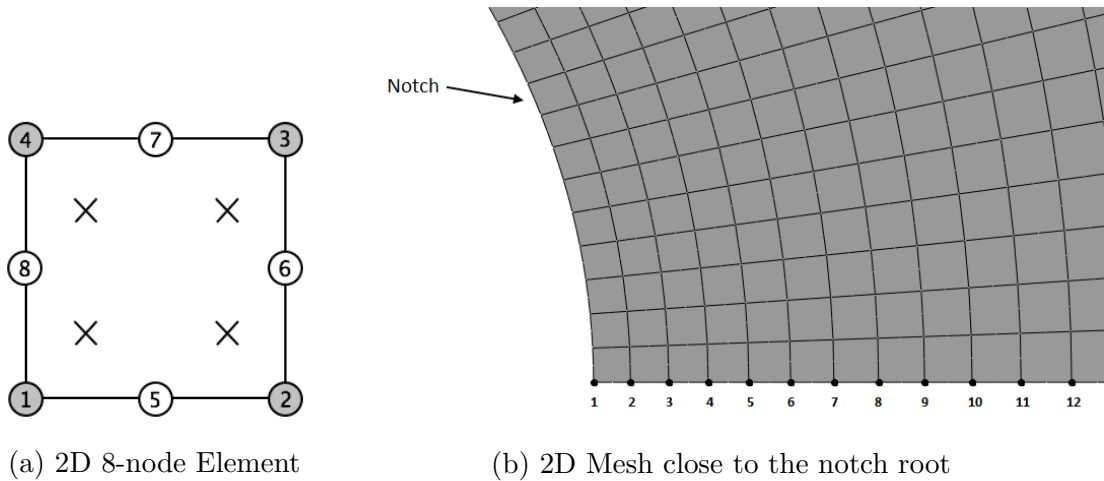


Figure 8: (a) The eight node element at the notch root, where the corner nodes are grey and crosses represent the *Gauss* points. (b) The 2D mesh closest to the notch-root, showing that node number 1 is the only node without shared boundaries.

*Gauss* integration points within the element for both two- and three-dimensional elements [13], as indicated by x-symbols in Figure 8a. Stresses calculated at the *Gauss* points are interpolated and extrapolated to all other points within the element, and the stress at any point within the element becomes a function of the stresses at the *Gauss* points [13].

The reason why the nodal stresses are less accurate is because the mesh consists of many elements that share the same boundaries, see Figure 8b. Stresses are discontinuous across these boundaries, as stresses change between elements [13]. This means that two neighbouring elements will predict different stress values at their connective nodes, as these values are based on extrapolations from the *Gauss* points within two different elements. This results in up to four different stress predictions at the same node.

The problem is usually solved by the FE software, that takes the average of these nodal stresses, and uses this average stress as the nodal stress [13]. Abaqus, which is the FE software used here, automatically averages the stresses if the node is shared by two or more elements [17]. Abaqus uses a 75% averaging threshold, meaning that the difference between the nodal solutions from all connected elements must be less than 25%. If not, then no data will be written for that particular node. Bell [13] argues that with a fine mesh, the actual resemblance between the element nodes are high, as the nodal stresses become very close to the stresses at the *Gauss* points. Thus, the problem of nodal averaging is likely to disappear with fine meshing.

Even with a fine mesh, the accuracy of the node at the notch root is a remaining

concern (see node number 1 in Figure 8b). As stresses at nodes shared between two or more elements are averaged, the node positioned at the notch root will not be averaged. This node is not shared with any other elements, as seen in Figure 8b. The stresses at this node are thus calculated using extrapolations within the element, so that the accuracy when using this node in finding the SCF and the stress gradient is unknown. In the following, the accuracy at this node is investigated, and different approaches to optimise the solution are suggested. One can assume that the FE-software describes the behaviour at node number 1 well, but as it is important that the SCF and the stress gradient is calculated as accurate as possible, it becomes vital to investigate this closely.

### 2.2.3 Finding the correct stress gradient from the FE-results

In the FEA post-processing stage it is possible to find the stress distribution close to the notch root of the structure and derive the stress function from it. The stress gradient can then be calculated from Eq.(6) by inserting the resulting stress and slope of the stress function at the notch root. In this case, if the nodal stress at the notch root is inaccurate, it affects the entire stress function, directly impacting both the SCF and the relative stress gradient.

A quick way to evaluate the accuracy of the stress function at the notch root is by studying the SCF at the notch root. This works as a first approach, because it is assumed that when the SCF is not calculated correctly, the stress gradient of the stress function must also be wrong. To demonstrate this approach, the FE-results for a 2D plate with an elliptic through-hole where  $b/a = 0.5$  was studied. Two different ways to find  $K_t$  was used, first by calculating  $K_t$  directly from the nodal stress at the notch root (node 1), and secondly by rejecting the node at the notch root and extrapolate polynomials from the nodal stresses at the other nodes (nodes 2, 3, ..., 8) to  $x = a$ . See Figure 8b for the nodal references. The results are presented in Figure 9, which is used as a first approach to consider the accuracy of the node at the notch root. If  $n$  is the number of nodes considered, a polynomial of  $n - 1$  degrees is used for all results, apart from the direct solution that is found at node 1. For the presentation of the results in Figure 9 a linear curve-fit is used between all of the  $K_t$  results, simply to visually enhance the results.

The SCF calculated directly from the nodal stress at node 1 is actually a very good result, as seen in Figure 9. Since the plate studied has a finite width  $a/w = 0.05$ , the analytical solution to the specific problem is unknown. The properties of  $K_t$  with increasing  $a/w$ , as previously presented, gives that the solution should be higher than the analytical solution. The element size itself,  $h/\rho = 0.041$ , also contributes to the elevation of the SCF relative to the analytical solution. The only other results from Figure 9 that seem to be of similar accuracy is when the first node is rejected and high order polynomials are applied, meaning that 6-7 nodes

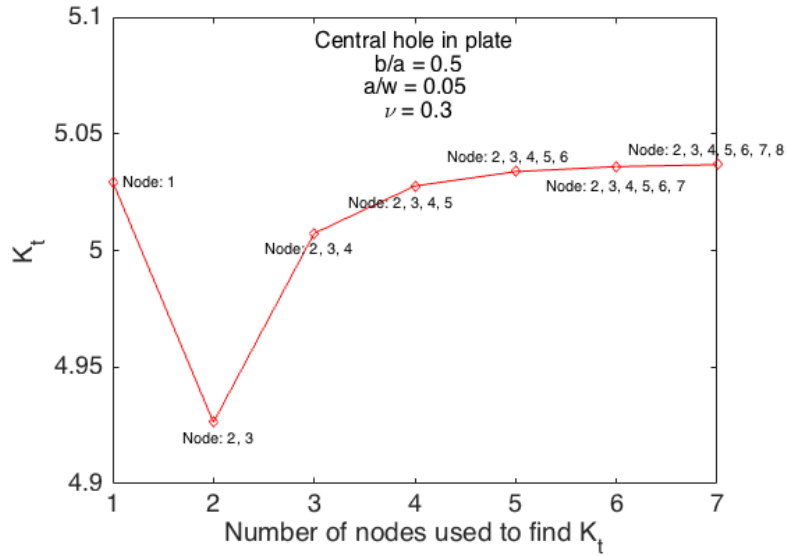


Figure 9: Difference in  $K_t$  at the notch root, when different nodes from the FE-solution are taken into consideration.

ahead of the notch are considered. This gives a converging SCF value, which is slightly higher than the value at node 1, but no conclusion as to which is more accurate can be made. These two solutions are very close to each other. For this thesis the required accuracy for fatigue applications was set to a maximum error of 1%, as errors lower than this will have little impact on the fatigue life, and both the results that were discussed lie below this error. For practical purposes, picking the nodal stress at node 1 is a much faster way to get results, and will be very beneficial for 3D FEA in particular. It is reasonable that by choosing this method to find the SCF, it provides great accuracy and the procedure is simple.

High accuracy predictions of the SCF is very important for relevant fatigue assessments, but it does not necessarily confirm that the stress function has the correct stress gradient. It is possible to achieve the same SCF value from functions with different stress gradients at the notch root. There is, however, only one gradient that is theoretically accurate, and it is important for correct fatigue assessments to get this property right.

In Figure 10 the stress gradient for a 2D plate with a circular through-hole ( $b/a = 1$ ) is presented and the same approaches, both including and rejecting node 1, are used to find the stress gradient. It is seen from the figure that the stress gradient increases when more nodes ahead of the notch are considered. When including node 1, the solution is almost exactly the same as when rejecting node 1, but only when considering the first two and three nodes away from the notch

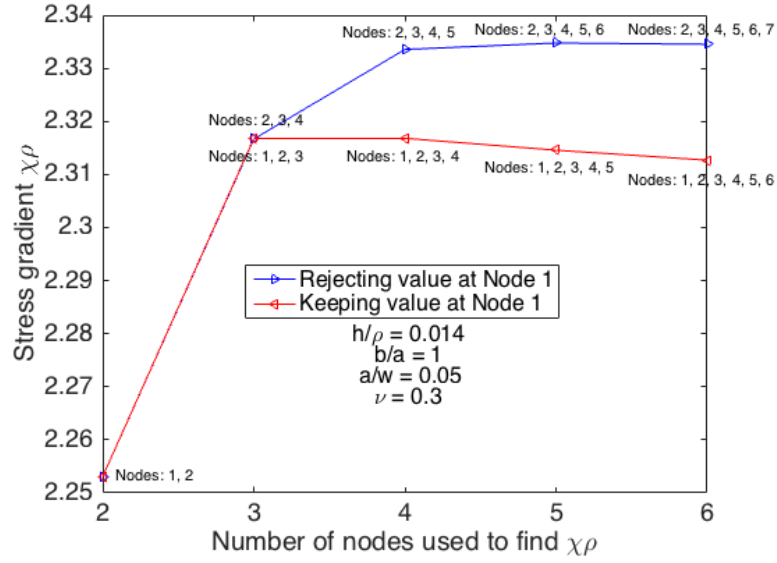


Figure 10: Stress gradient at the notch root ( $x = a$ ) of a circular hole in a plate, where the number of nodes considered determines the solution.

root. When including more than the three first nodes (nodes 1-3), the solution decreases slightly as the number of nodes increases. When node 1 is rejected, the stress gradient continues to increase until five nodes ahead of the notch are considered (nodes 2-6), and from this point it becomes constant.

The analytical solution for the stress gradient at a circular hole is  $\chi\rho = 7/3$ , but that is for an infinitely wide plate and the effect of  $a/w$  and  $h/\rho$  on the solution is unknown, as it is not documented in literature. Hence, the results in Figure 10 are not expected to reach the analytical solution. The solutions both involving and excluding node 1, separate when considering more than three nodes, but it is not yet known which of these that is the most accurate solution. In order to make any further statements about whether to include the first node or not, an investigation of the impact of  $h/\rho$  and  $a/w$  on the stress gradient is included.

Figure 11 and Figure 12 show how the stress gradient changes with  $h/\rho$  and  $a/w$  respectively. In these figures the solutions are extrapolated to  $h/\rho = 0$  and  $a/w = 0$ . The results in Figure 11 are from an FEA where  $a/w = 0.05$ , and the results in Figure 12 are from an FEA where  $h/\rho = 0.04$ , so that the analytical solution is not expected in either of these cases. However, a combination of these graphs where both  $h/\rho$  and  $a/w$  goes to zero should lead to the analytical solution. As the solution that includes node 1 is already below the analytical solution when  $h/\rho = 0$  in Figure 11, and according to Figure 12 is expected to continue to decrease with decreasing  $a/w$ , this solution is not approaching the analytical solution.

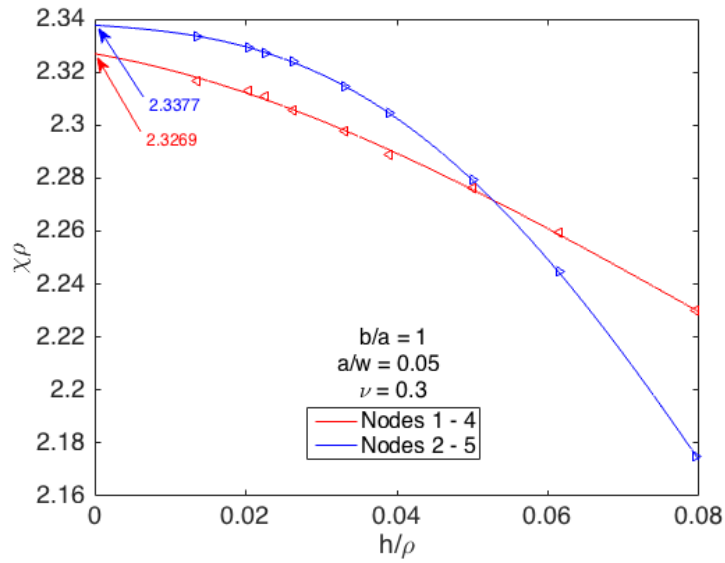


Figure 11: The stress gradient solution for varying  $h/\rho$  from 2D FEA of a plate with a central circular hole, comparing the results from nodes 1 – 4 and 2 – 5.

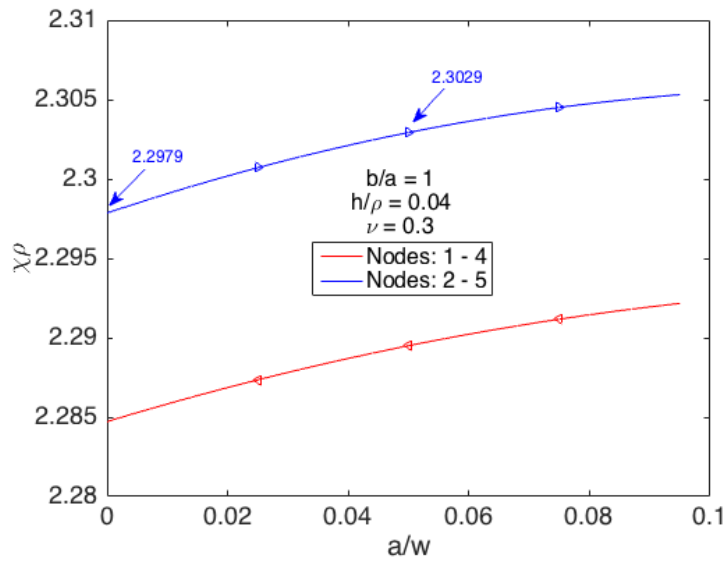


Figure 12: The stress gradient solution for varying  $a/w$  from 2D FEA of a plate with a central circular hole, comparing the results from nodes 1 – 4 and 2 – 5.

When considering the combination of figures for the stress gradient calculated from nodes 2-5 instead, the anticipated result becomes  $\chi\rho = 2.3327$  as  $h/\rho = a/w = 0$ , which is very close to the analytical value. From this, it is clear that the stress gradient is best determined from nodes 2-5, which will be used throughout this thesis. It could be argued that choosing nodes 2-6 could lead to a slightly more accurate solution based on what was shown in Figure 10. Due to a desire to keep the number of nodes to an absolute minimum, in order to manage the workload during post processing of all FEAs, nodes 2-5 is a better choice in this thesis, as the accuracy is still extremely close to the solution with nodes 2-6.

As the stress field close to the notch root undergoes a rapid increase, caused by the notch, this region is dominated by high stress gradients. It is seen from Figure 11 that the mesh density in this region, close to the notch root, clearly affects the accuracy of the results. Unfortunately, even with today's powerful computers, it is difficult to overcome this effect, as computational time is so demanding for 3D models. The lowest mesh density that was possible with 3D FE-models for this thesis was  $h/\rho = 0.06$ , which means that a negative error of about 4% might be expected for the stress gradient results. A lower stress gradient is more critical for fatigue, and the error leads to a conservative fatigue assessment.

### 2.3 Stress concentration at side-grooves in plates

As 2D FE-models solve quickly with today's computers, it is an excellent way to test a broad range of properties and learn as much as possible about the stress behaviour, and thorough testing of the accuracy is possible. A 2D model of a plate with a central hole has a lot of similarities with a 2D model of a plate with side-grooves. In fact, the modelling procedure in FEM only requires the changing of one boundary condition to make a plate with side-grooves from a plate with a central hole. Because of this, it is very natural to also test the accuracy of 2D plates with side-grooves in order to investigate the accuracy of FEA properly. The principle difference between the SCFs for central holes and side-grooves is also a very central part of the theory on SCFs. A short presentation of the SCF behaviour for plates with side-grooves hence serve the purpose of demonstrating important principles from theory as well as investigating accuracy.

Unfortunately, analytical solutions are not widely available for plates with side-grooves in the same manner as for central holes. However, several equations are presented in literature that are based on numerical approaches and physical tests. These equations are widely accepted and it is expected that the FE-results, with the desired accuracy, should deviate less than 1% from the equations.

### 2.3.1 Semicircular side-grooves

Several equations for plates with semi-circular side-grooves are found in literature. The equations presented by Roark [5] and Pilkey [6] are slightly different, but they give the same result for a finite width plate with semicircular side-grooves. The equation as presented by Roark [5] is:

$$K_t = \frac{1}{1 - \left(\frac{a}{w}\right)} \left[ 3.065 - 3.37 \left(\frac{a}{w}\right) + 0.647 \left(\frac{a}{w}\right)^2 + 0.658 \left(\frac{a}{w}\right)^3 \right] \quad (7)$$

where the term outside the square brackets is the geometric relation between the net section and the gross section of the structure, as only the gross SCFs is considered in this thesis, for simplicity.

When  $a/w = 0.05$  Eq. (7) gives  $K_t = 3.05$ . In comparison, a 2D FEA for a plate with semicircular side-grooves gives  $K_t = 3.067$ . Here the FE-result is 0.56% higher than the result from Eq. (7). The same mesh was used for the plate with side-grooves as for a central hole, and it is evident that the accuracy of the FEA relative to Eq. (7) is very good. It is also emphasised by both Roark [5] and Pilkey [6] that Eq. (7) gives excellent agreement with test-data when  $a/w \leq 0.5$ .

If comparing the results for side-grooves with the corresponding solutions for central holes, it is observed that side-grooves cause higher SCFs, and the explanation is that these two models have different constraints. As already shown, the central hole causes a maximum tensile stress of approximately  $\sigma_y = 3S$  at the notch root, but it also causes a compressive stress in  $x$ -direction  $\sigma_x = -S$  above and below the hole. The same behaviour is not possible for a plate with side-grooves, where stresses in  $x$ -direction above/below the semicircle would act perpendicular to a free surface, thus must be zero due to mechanical equilibrium. In order to balance the compressive stress above/below the central hole, moments are initiated. These moments cancel out, but they constrain the material above/below the circular hole if compared to side-grooves. Thus giving an explanation as to why the SCF is higher for side-grooves than central holes.

### 2.3.2 Semi-elliptic side-grooves

Plates with semi-elliptic side-grooves are not covered in engineering handbooks, but Peterson [6] showed that central elliptic holes and central U-shaped holes give SCFs with a difference of about 2%. Based on this, it is reasonable to assume a similar relation between semi-elliptic side-grooves and U-shaped side-grooves. With the same mesh as for central elliptic holes, a similar accuracy is expected. 2D FEA gave  $K_t = 5.235$  for a plate with semi-elliptic side-grooves, when  $\rho = 1.25$  and  $a/w = 0.05$ .

### 2.3.3 U-shaped side-grooves

In order to compare the FEA results for semi-elliptic side-grooves with literature, the available equations for U-shaped side-grooves are needed. Together with the equation for semicircular side-grooves in plates, Pilkey [6] and Roark [5] also present equations for U-shaped side-grooves. The equation for U-shaped side-grooves when the curvature at the notch root is  $\rho = 1.25$ , based on the presentation by Roark [5], is:

$$K_t = \frac{1}{1 - \left(\frac{a}{w}\right)} \left[ 4.935 - 4.878 \left(\frac{a}{w}\right) + 0.515 \left(\frac{a}{w}\right)^2 + 0.432 \left(\frac{a}{w}\right)^3 \right] \quad (8)$$

which, just like for semicircular side-grooves, gives the gross SCF.

When inserting  $a/w = 0.05$ , Eq. (8) gives  $K_t = 4.939$ . The result is questionable straight away, as the result is below the analytical SCF for a central elliptic hole. It turns out, by consulting the corresponding chart developed by Peterson [6], that the solution for U-notches becomes asymptotic as the ratio  $\rho/(w - a)$  becomes significantly small. For this thesis, the value is extremely small, and not covered by the chart. Hence, it becomes reasonable to assume that the equation is invalid for the specific case studied.

If considering the same example using FEA,  $K_t = 5.36$  for a plate with U-shaped side-grooves. When comparing the FE-results for U-shaped side-grooves and semi-elliptic side-grooves, the difference is 2.4%. The correspondence between the FE-results is very consistent, as Peterson [6] suggested a difference of 2% for central elliptic and central U-shaped holes. The general accuracy of the FE-model has shown to be very high to this point, and it is most likely to be within 1% error of the potential analytical solution.

The FE-results show great consistency, where the SCF increases as expected when going from a plate with semi-elliptic side-grooves to a plate with U-shaped side-grooves. Also, the FE-results provided great accuracy for the plate with semicircular side-grooves. There is no doubt that FEA is a powerful tool as it has shown a consistent and high accuracy, throughout the preliminary study.



## 3 2D FEA used for 3D evaluation of structures

It is commonly assumed that 3D FEA best describes real structures, but some methods exist to calculate 3D behaviour from simple 2D FE models. Two cases that will be studied in the following are 2D axisymmetric models of cylinders and 2D models of plates in plane strain. Plane strain is the theoretical state of a plate when it has infinite thickness, and 2D plane strain models can thus approximate the behaviour of plates with large thicknesses. 2D models of axisymmetric cylinders on the other hand, is the most conventional and accurate way to model cylinders that have one axis of symmetry, as well as being a simple method that is quickly performed.

Recent literature points at four important impacts on the maximum SCF in three-dimensional structures. These are the thickness of the plate, the Poisson's ratio of the material, the width of the plate and the notch shape. These findings are credited to She and Guo [7], Yu et al. [8], Vaz et al. [9] and Yang et al. [18]. The 2D FEA of plates in this section focuses on plates with a central circular hole, and because the plate width is constant ( $a/w = 0.05$ ) and the thickness is infinite (plane strain), the effect of the Poisson's ratio on  $K_t$  and the stress gradient is what will be studied closely. To find the effect of thickness on  $K_t$  and the effect of Poisson's ratio on plates with different thicknesses, 3D FEA is required. For the 2D FE study of axisymmetric cylinders, the cylinder radius is constant ( $a/w = 0.05$ ), but the effect of both the notch shape and the Poisson's ratio will be studied.

### 3.1 Theoretical approach to plane strain

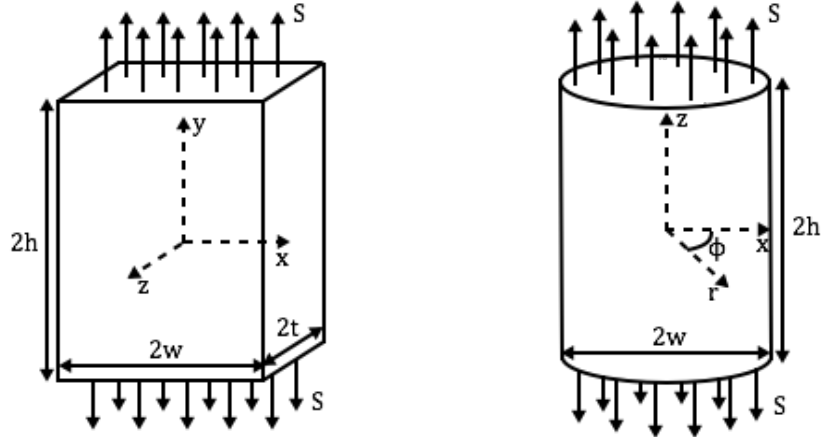
#### 3.1.1 Hooke's law

For this thesis, only isotropic linear-elastic materials are considered. An isotropic material has the same properties in all directions within the material [19], and linear-elastic materials have a linear relationship between stresses and strains, where the strain returns to zero upon unloading [20]. Hooke's law describes the linear relation between stress and strain [2]. If a structure is loaded in uni-axial tension in the  $y$ -direction, see Figure 13a, the elastic elongation by Hooke's law is

$$\varepsilon_y = \frac{\sigma_y}{E} \quad (9)$$

where  $E$  is the Young's Modulus of the material.

When the structure is subjected to loading in one direction, it affects the material behaviour in the other two directions as well. The Poisson's ratio is the ratio between the transverse strain and the axial strain [2], given as



(a) Cartesian coordinate system. (b) Cylindrical coordinate system.

Figure 13: The difference between the coordinate systems for plates and cylinders.

$$\nu = -\frac{\varepsilon_z}{\varepsilon_y} \quad (10)$$

where  $\varepsilon_z$  is the transverse strain through the thickness of the structure (the  $z$ -direction). The same equation can be found for the strain in  $x$ -direction simply by replacing  $\varepsilon_z$  with  $\varepsilon_x$ .

From Eq. (9) and Eq. (10) it is found that two independent elastic constants are needed to characterise the isotropic linear-elastic material [20], the Young's Modulus  $E$  and the Poisson's ratio  $\nu$ .

In this section, all equations are presented using Cartesian coordinates, simply for brevity. Figure 13b shows the cylindrical coordinate system within a cylinder, which can be compared to the Cartesian coordinates as shown in Figure 13a. The concern is that by including cylindrical coordinates, it could lead to confusion as the axial strain for cylinders is labelled  $\varepsilon_z$ . Further, the transverse strains in the cylinder consist of the circumferential strain  $\varepsilon_\phi$  and the radial strain  $\varepsilon_r$ . The cylindrical coordinates will however be used when considering 2D axisymmetric cylinders, but only then.

When giving Eq. (10) a closer look, it gives negative transverse strains, as the Poisson's ratio is positive for most materials [20]. This means that while the structure is elongated in the  $y$ -direction, the structure has a contraction in the two other directions [2]. The transverse strains can be expressed in terms of the applied stress  $\sigma_y$ , as follows:

$$\varepsilon_x = \varepsilon_z = -\nu \frac{\sigma_y}{E} \quad (11)$$

where the transverse strains are equal because the material is isotropic.

If the plate, or even just an infinitesimal piece of the material, is loaded in three directions, the coupling between all three contributions can be found by superposing the strains [2] so that

$$\begin{aligned}\varepsilon_x &= \frac{1}{E}[\sigma_x - \nu(\sigma_y + \sigma_z)] \\ \varepsilon_y &= \frac{1}{E}[\sigma_y - \nu(\sigma_x + \sigma_z)] \\ \varepsilon_z &= \frac{1}{E}[\sigma_z - \nu(\sigma_x + \sigma_y)]\end{aligned}\tag{12}$$

which ultimately leads to a 3D version of Hooke's law.

### 3.1.2 Plane strain

An infinitely thick plate is, by definition, in plane strain (PE) [2]. With PE, it follows that there are no out-of-plane strains, so that  $\varepsilon_z = 0$ . Even though an infinite thickness is purely theoretical, the PE solution is often used as an approximate for plates with a very large thickness compared to all the other dimensions. If inserting the PE condition  $\varepsilon_z = 0$  into Eq. (12), it gives:

$$0 = \frac{1}{E}[\sigma_z - \nu(\sigma_x + \sigma_y)]$$

and by re-arranging the equation, it is found that

$$\sigma_z = \nu(\sigma_x + \sigma_y)\tag{13}$$

when a structure is in plane strain.

Eq. (13) shows that the stress appearing in the thickness-direction is a function of the in-plane stresses,  $\sigma_x$  and  $\sigma_y$ . At the notch root  $\sigma_x = 0$  and  $\sigma_y$  reaches its maximum value, and the stress in  $z$ -direction simplifies to

$$\sigma_z = \nu\sigma_{y,\max}\tag{14}$$

giving a linear relationship between the stress in the loading direction and the thickness direction for plates in plane strain. As seen, the ratio between these stresses is given by the Poisson's ratio of the material.

### 3.1.3 Generalised plane strain

The plane strain approach involves a plate with infinite thickness and no out-of-plane strain. The general plane strain (GPE) approach suggests that the out-of-plane strain reaches a constant ( $\varepsilon_z = \text{constant}$ ), rather than go to zero, when

a certain plate thickness is reached [2]. Such behaviour is more realistic, as an infinite thickness is not achievable for real structures.

In order for the material to have constant strain in  $z$ -direction, the strain far away from the notch root must equal the strain at the notch root. The strain far away from the notch root can be found by rewriting the expression for  $\varepsilon_z$  found in Eq. (12). If considering the strain at the gross section of the plate,  $\sigma_y = S$  while  $\sigma_x = \sigma_z = 0$ , so that

$$\varepsilon_{z\infty} = -\nu \frac{S}{E} \quad (15)$$

where  $\varepsilon_{z\infty}$  refers to the strain at the gross section, where the stress is applied.

As already mentioned, the condition for GPE requires that the remote strain equals the strain at the notch root, which can be expressed as follows:

$$\varepsilon_z = \varepsilon_{z\infty}$$

which means that Eq. (15) gives the constant strain required for GPE.

Inserting the expression for constant strain into Eq. (12), the stress at any point inside the material can be calculated. The notch root is the most interesting point to study, due to the high stress concentration, and here  $\sigma_x = 0$ . The equation for  $\varepsilon_z$ , as taken from Eq. (12), reduces to:

$$-\nu \frac{S}{E} = \frac{1}{E} [\sigma_z - \nu \sigma_y]$$

If rearranging the variables, the equation for the stress in thickness direction under GPE is found:

$$\sigma_z = \nu(\sigma_y - S) = \nu(K_t - 1)S \quad (16)$$

which depends on  $K_t$  (the SCF in  $y$ -direction) and the Poisson's ratio.

## 3.2 2D FEA of plates in plane strain

The FE-software is able to give solutions for plates with infinite thicknesses, simply by changing the element settings to plane strain (PE). The element settings can also be set to generalised plane strain (GPE), which is the expected behaviour when plates reach a certain finite thickness. In this section, both these features will be utilised and the results are compared. These features are valuable options to 3D FEA, as 3D models often require extreme computation time. The actual change in SCF with increasing thickness is studied by 3D FEA in a later section, where the solution approaches GPE as the thickness increases.

### 3.2.1 Central circular holes

The results from 2D FEA for plates with a central circular hole with varying Poisson's ratio is presented in Figure 14. Figure 14a shows the behaviour in PE and Figure 14b shows the behaviour in GPE. It turns out that the in-plane stresses for infinitely thick plates are the same as for thin plates (in PS), but with an additional stress component in the thickness direction.  $K_t$  in Figure 14a, called  $K_{ty}$  to avoid confusion, is the same value that was found for thin plates in the preliminary study.

When the plate is in GPE the value of  $K_{ty}$  is slightly higher, but in both cases unaffected by varying Poisson's ratio. The SCF in the thickness direction,  $K_{tz}$ , is the only component that changes with Poisson's ratio, where the effect is highest for PE. The difference between the solutions in PE and GPE is small for  $K_{ty}$ , but high for  $K_{tz}$ . This is expected, as GPE is more trusted than PE in replicating the real thickness-effect on structures.

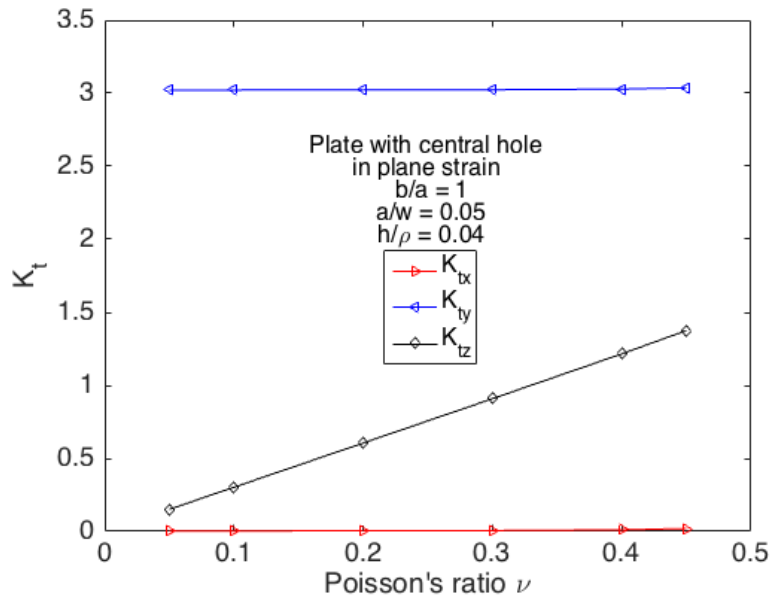
The dependence between the through-thickness stress and the Poisson's ratio under PE was shown in Eq. (14), where  $K_{tz}$  is the product between  $K_{ty}$  and  $\nu$ , which is also visible when studying the results in Figure 14 closer. The equation for the through-thickness stress under GPE was shown in Eq. (16), which directly explains why the GPE results give a lower SCF. As  $K_{tz}$  is given by  $\nu(K_{ty} - 1)$ , which is the result for PE minus the Poisson's ratio. The relationship is visible if comparing Figure 14a and Figure 14b. It is also seen in the figures that  $K_{tx} = 0$ , as stress perpendicular to a free surface must be zero, so that there can be no stresses acting in the  $x$ -direction at the notch root.

The use of 2D FEA and GPE will be further studied by looking at the results for semicircular side-grooves in plates. These results will be compared with the behaviour of cylinders, used to evaluate the accuracy of the results.

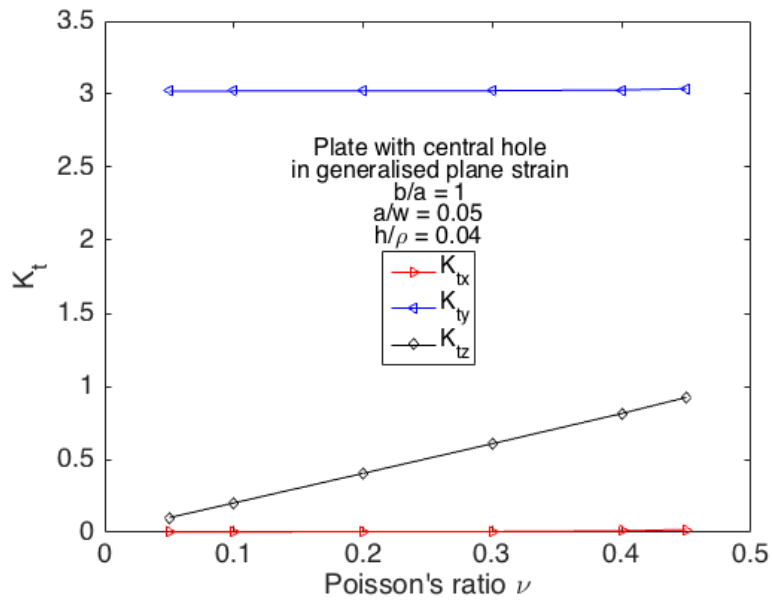
### 3.2.2 Semicircular side-grooves

In the preliminary study it was shown that plates with side-grooves cause higher SCFs than plates with central holes, and that this was due to a difference in constraints. Thus, it is interesting to further evaluate the behaviour of plates with side-grooves, also because these results can be compared to cylinders with circumferential grooves, which is a very common design.

The results from FEA for plates with semicircular side-grooves are shown in Figure 15. Figure 15a shows the results when the plate is in PE and Figure 15b shows the results for GPE. Immediately it is seen that the results are very similar to those for central circular holes, where the only difference is that the stresses are slightly higher. This observation is true because  $K_{ty}$  is higher for plates with side-grooves, as already shown in the preliminary study, and due to Eq. (14) and

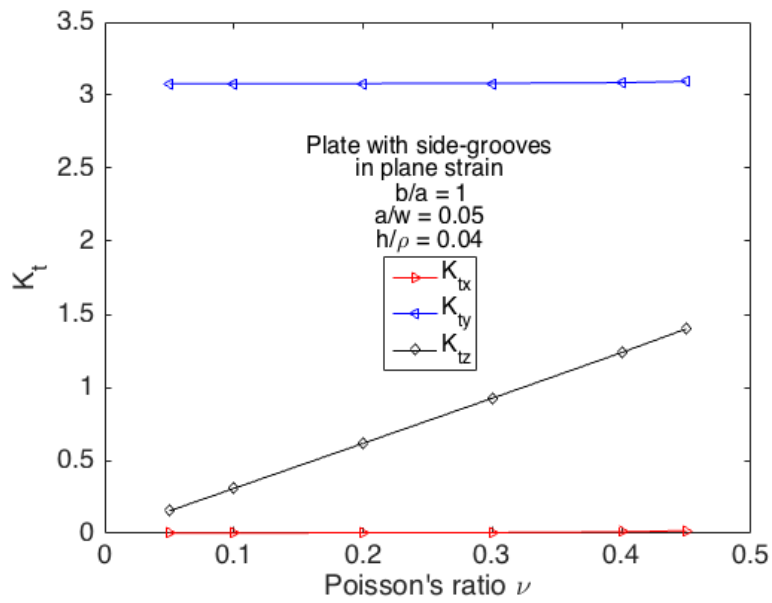


(a) Plane strain

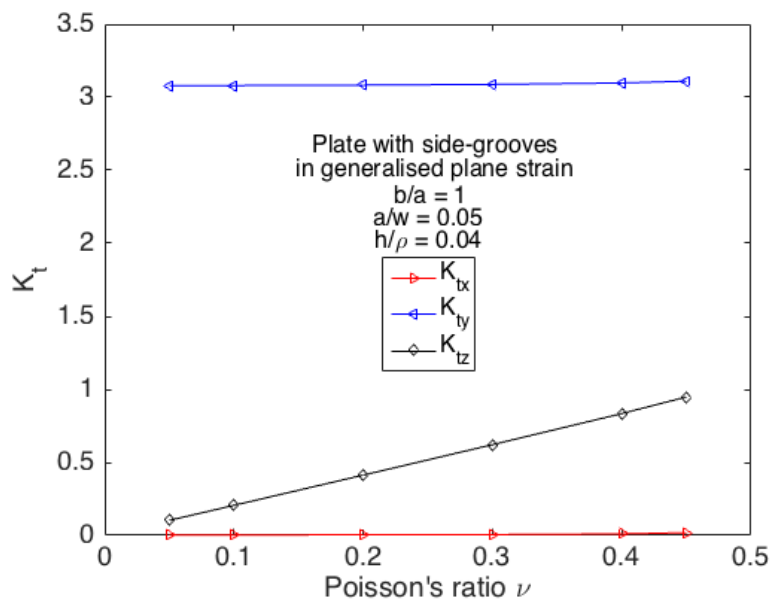


(b) Generalised plane strain

Figure 14: Results from FEA for a plate with a central circular hole when the plate is in a) plane strain and b) generalised plane strain.



(a) Plane strain



(b) Generalised plane strain

Figure 15: Results from FEA for a plate with semicircular side-grooves when the plate is in a) plane strain and b) generalised plane strain.

Eq. (16) the through-thickness SCF depends on  $K_{ty}$  and increases accordingly. Apart from this, the relationship between the SCF for PE and GPE is the same as for plates with central holes, as the same equations (Eq. (14) and Eq. (16)) apply.

### 3.3 3D cylinders from 2D axisymmetric FE-models

Even though cylinders are three-dimensional structures, they have an axisymmetric property that makes FE-modelling very simple. In fact, the complete 3D behaviour of cylinders can be found from a 2D axisymmetric model. What this means is that the cross section of the structure can be modelled, and by applying a rotational symmetry to one of the edges, the FEA understands the full extent of the problem and gives 3D results. In combination with the results for plates in GPE, it provides a good outlook on the properties of SCFs and the stress gradient. In particular, the behaviour related to the transverse/circumferential material contraction.

A special mesh, using axisymmetric elements, is applied to achieve the correct results. Apart from this, the same meshing technique as for plates can be applied, as both  $\rho$  and  $a/w$  are unchanged. The mesh sensitivity towards notch shape and finite width was shown in the preliminary study, and as long as these are considered it is reason to trust that the accuracy is maintained.

#### 3.3.1 Central spheres and spheroids

Analytical equations for stresses at central spheres in cylinders are presented both by Timoshenko and Goodier [2], and by Barber [4]. Both approaches give the same solution at the notch root of the sphere. The analytical equations, as presented by Timoshenko and Goodier [2], are:

$$\frac{\sigma_r}{S} = -\frac{6}{7-5\nu}\left(\frac{a}{r}\right)^5 + \frac{6}{7-5\nu}\left(\frac{a}{r}\right)^3 \quad (17)$$

$$\frac{\sigma_z}{S} = \frac{9}{2(7-5\nu)}\left(\frac{a}{r}\right)^5 + \frac{4-5\nu}{2(7-5\nu)}\left(\frac{a}{r}\right)^3 + 1 \quad (18)$$

$$\frac{\sigma_\phi}{S} = \frac{3}{2(7-5\nu)}\left(\frac{a}{r}\right)^5 - \frac{6-15\nu}{2(7-5\nu)}\left(\frac{a}{r}\right)^3 \quad (19)$$

where  $r$  is the cylindrical coordinate in the radial direction, see Figure 13b, away from the centre of the sphere so that  $r = a$  is at the notch root.

Furthermore, an analytical solution for the stresses at spheroids ( $b \neq a$ ) in infinite bodies was developed by Neuber [3], and a chart based on these results is found in Peterson [6]. The actual presentation of Neubers analytical equations in «Theory of Notch Stresses» [3] is too comprehensive to consider here. However,



Neuber's approach began by finding the solution for a spherical hole [3], and his equations give the same stresses at the notch root as Timoshenko and Goodier [2].

Since  $r = a$  at the notch root of the sphere, the stress concentration factors acting in all three directions at the notch root can be found from Eqs.(17)-(19). The SCF at the notch root of a central sphere in a cylinder can be found from

$$K_{tz} = \frac{27 - 15\nu}{2(7 - 5\nu)} \quad (20)$$

$$K_{t\phi} = \frac{15\nu - 3}{2(7 - 5\nu)} \quad (21)$$

$$K_{tr} = 0$$

for any given Poisson's ratio.

If  $\nu = 0.3$ ,  $K_{tz} = 2.045$ , which is considerably lower than the theoretical SCF for a circular hole,  $K_t = 3$ . This observation is well known and reasonable because the stress can redistribute about the circumference of a sphere more smoothly than about a hole constrained by two free plate-surfaces. The radial stress is zero, as its direction is perpendicular to the hole.

Eqs.(20)-(21) show that the SCF for a sphere depends on the Poisson's ratio, and in Figure 16 these equations are plotted together with the results from a 2D FEA, to show the effect of Poisson's ratio. In Figure 16, the FEA results and the analytical solution are in complete agreement. The circumferential SCF,  $K_{t\phi}$ , increases with increasing Poisson's ratio, as was also observed in the thickness-direction of plates in PE and GPE.

The FE-results for the SCF in the loading direction of cylinders,  $K_{tz}$ , for spheres ( $b/a = 1$ ) and spheroids ( $b/a = 0.5$  and  $b/a = 2$ ) are presented in Table 2. The SCF increases with decreasing radius of curvature at the notch root, which is consistent with the theory for plates [1]. The analytical solution for a central sphere is also presented in Table 2, showing a deviation of 0.025% for the FE results. This deviation is very small, again confirming the high accuracy of the FE-model. The accuracy for a cylinder with a central spheroid is assumed to be within a similar accuracy, as the same mesh with  $h/\rho = 0.04$  is used. The chart presented in Peterson [6] confirms that the FE-results for spheroids are close, but the accuracy cannot be confirmed as the chart does not cover the relevant region in detail.

The analytical stress gradient at the notch root of a sphere can be calculated from the stress distribution in Eq.(18), as given by Timoshenko and Goodier [2], by using the equation for the relative stress gradient Eq. (6). In Figure 17 the analytical result is compared to the stress gradients calculated from the FE-results, by using the method developed in the preliminary study. The stress gradient is

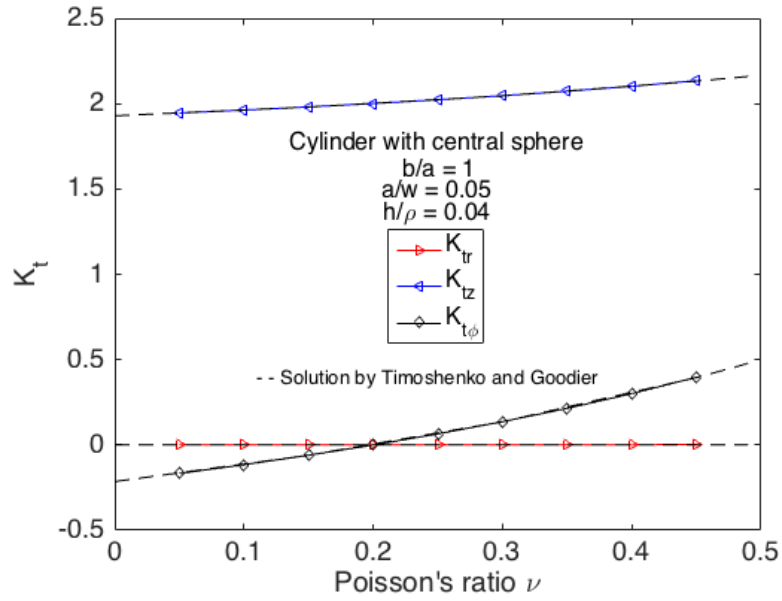


Figure 16:  $K_t$  results from FEA for a cylinder with central sphere for changing Poisson's ratio, compared to the solution by Timoshenko and Goodier [2].

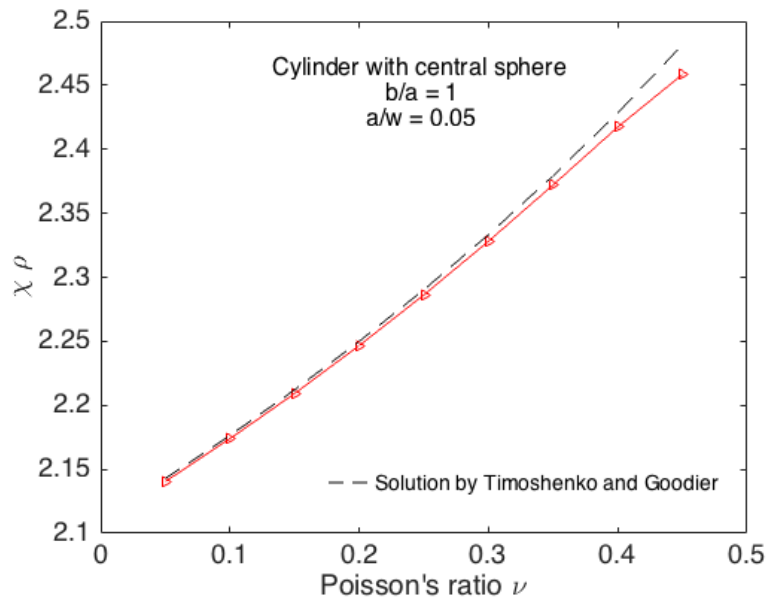


Figure 17: The stress gradient  $\chi\rho$  at the notch root of a central sphere with changing Poisson's ratio. The stress gradient found from the analytical solution by Timoshenko and Goodier [2] is also presented.

Table 2:  $K_t$  from FEA for spheroidal cavities in cylinders with varying notch shape, compared with the analytical solution by Timoshenko and Goodier [2].

	b/a = 0.5	b/a = 1	b/a = 2
$K_{tz}$ from FEA	3.32321	2.04448	1.44105
$K_{tz}$ from [2]	-	2.045	-

the same as for a circular through-hole in a plate, giving  $\chi\rho = 7/3$  when  $\nu = 0.3$ . The figure shows that the accuracy of the FEA is great, as the result is almost exact. For large Poisson's ratios there is a small difference between the results, but this is the region with highest stress gradients, and a slight deviation is not surprising. Overall, the FEA gives almost perfect accuracy compared to the available analytical solutions, both for the SCF and the stress gradient.

### 3.3.2 Circumferential grooves

Analytical solutions to circumferential grooves are not available in literature, but it should be mentioned that Neuber [3] developed a theoretical solution for deep hyperbolic circumferential grooves. As these solutions are extensive, and not relevant to the shapes studied here, no further details are presented. However, based on the results, Neuber developed an equation (see Peterson [6] pg.59) which he suggested to use as an approximate for grooves of arbitrary shapes. Peterson [6] applied this equation to produce a chart of approximated SCFs for U-shaped circumferential grooves in cylinders. Based on this, Roark [5] presents the following approximate equation for semicircular grooves in cylinders:

$$K_t = \frac{\pi w^2}{\pi(w-a)^2} \left[ 3.04 - 5.42 \left( \frac{a}{w} \right) + 6.27 \left( \frac{a}{w} \right)^2 - 2.89 \left( \frac{a}{w} \right)^3 \right] = 3.085 \quad (22)$$

where the fraction outside the square brackets turns the result into a gross SCF.

When  $a/w = 0.05$ , the result from Eq. (22) is  $K_t = 3.085$ . From FEA of cylinders with semicircular circumferential grooves,  $K_t = 3.142$  was found. Thus the FEA gives a 1.85% error relative to Roark's solution. The accuracy is expected to be much higher when compared to an analytical solution of the problem, as the FE-model is the exact same one as was used for central spheres. The only difference is that one boundary condition is changed. This means that the same mesh is used, where  $h/\rho = 0.04$ . This model provided great accuracy for cylinders with central spheres, where the results were almost equal to the analytical solution. The results found from FEA for circumferential grooves rises a concern about the accuracy of Roark's solution, and further comparison to Eq. (22) becomes less relevant.

Table 3:  $K_t$  from FEA for circumferential grooves in cylinders with varying notch shape, compared to available solutions in literature [5].

	$b/a = 0.5$	$b/a = 1$	$b/a = 2$
$K_t$ FEA	5.38474	3.14239	2.06185
$K_t$ [5]	-	3.085	-

Figure 18 presents the FE-results for cylinders with semicircular circumferential grooves and the effect of Poisson's ratio on the results. From the figure it is observed that the SCF in the circumferential direction ( $K_{t\phi}$ ) increases with increasing Poisson's ratio, while the SCF in the loading direction ( $K_{tz}$ ) slightly decreases. In comparison to the results for central spheres,  $K_{t\phi}$  is significantly higher for circumferential grooves and the effect of Poisson's ratio is stronger. It is also found that  $K_{tz}$  is higher for circumferential grooves than it is for central spheres, which is caused by the strong radial contraction of the cylinder. This causes a bottleneck in the stress distribution through the cylinder, causing abrupt changes, and an elevated stress concentration is the result. This elevated value is very close to the SCF for plates with side-grooves, and this similarity is further investigated in the next section.

To compliment the semicircular FE-results, two other notch shapes were studied. In Table 3 all SCF results from FEA for cylinders with circumferential grooves are presented. The Poisson's ratio  $\nu = 0.3$  for all these analyses. The table also includes the solution from Roark [5]. It was desired to compare Roark's equations for U-shaped circumferential grooves to the FE-results for semi-elliptic grooves as well, but these equations were not valid for the cases studied here.

Accompanied by higher SCFs than for central spheres, the stress gradients are lower for most Poisson's ratios as well. This means that the region of highly stressed material is much higher for cylinders with circumferential grooves, which is known from theory [16]. The behaviour of the stress gradient for semicircular grooves is presented in Figure 19, and the results are calculated based on the stress distributions found from FEA. The stress gradient when  $\nu = 0.3$  can be found from Figure 19, giving  $\chi\rho = 2.239$ .

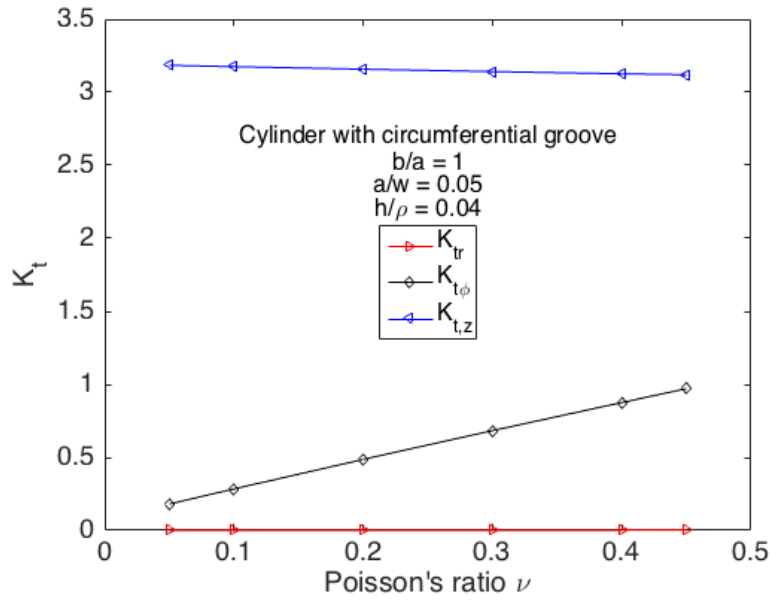


Figure 18:  $K_t$  results from FEA for a cylinder with semicircular circumferential groove for changing Poisson's ratio.

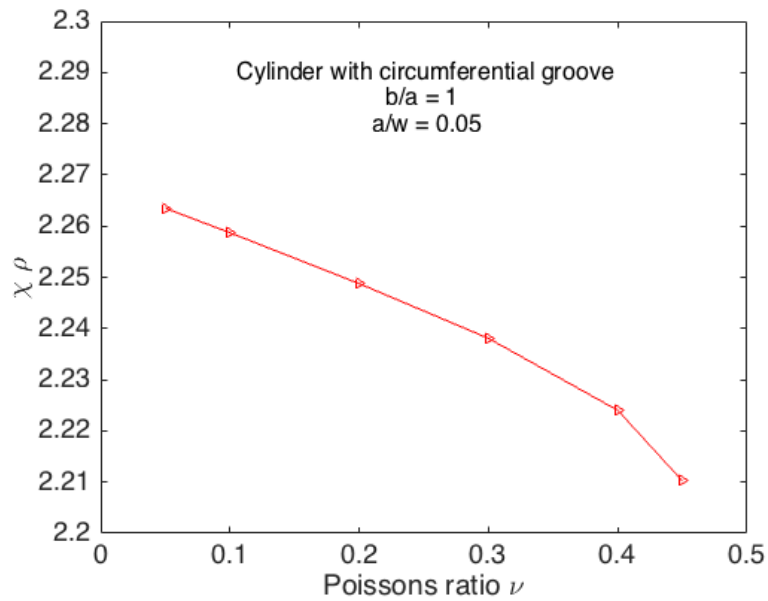


Figure 19: The stress gradient  $\chi_\rho$  at the notch root of a cylinder with semicircular circumferential groove, with changing Poisson's ratio.

### 3.4 Similarities between cylinders and plates in GPE

It was previously shown that plates in PE and GPE gave different estimations of the SCF, and it was mentioned that GPE was the most realistic approach. It is assumed that an FE-model in GPE gives a good description of the stress acting in the thickness-direction. The FE-results for plates and cylinders can be used to prove this assumption. The thickness direction of plates and the circumferential direction of cylinders will here be generalised as the «transverse direction».

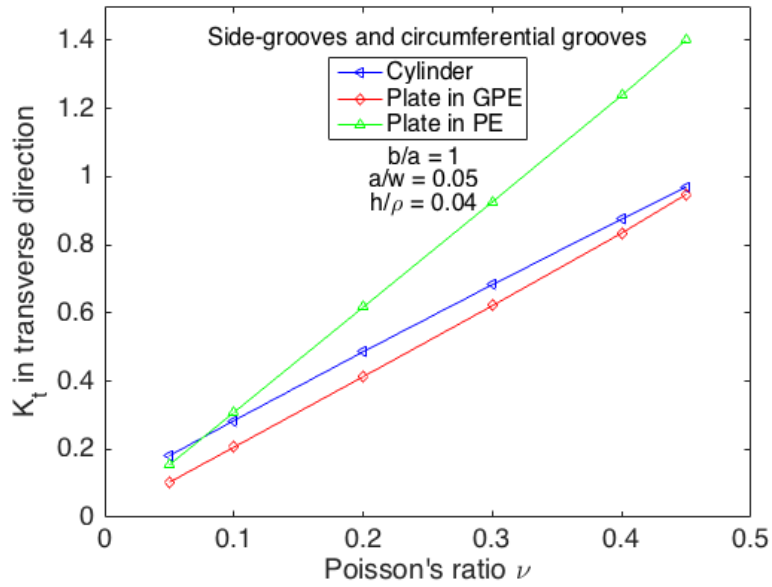
Figure 20a compares the results for transverse stresses in plates with side-grooves (both in PE and GPE) and cylinders with circumferential grooves. It is seen that the plate in GPE gives a very similar result as the cylinder. The explanation is that when a plate is thick enough, it will be difficult for the material to know whether it is inside a plate with side-grooves or inside a cylinder with a circumferential groove. For plates with a certain thickness, the material is assumed to reach GPE, where the through-thickness strain is constant. For cylinders, the strain in the circumferential direction is also constant, due to the rotational symmetry. The conclusion from this is that a plate with side-grooves in GPE and a cylinder with a circumferential groove behave similarly.

The geometries of the two cases are also related, as the cross section of the cylinder with a circumferential groove makes an exact 2D plate with side-grooves. This is why the SCFs in loading direction are also similar. From FEA, where  $\nu = 0.3$ ,  $K_t = 3.088$  for the plate in GPE and  $K_t = 3.141$  for the cylinder.

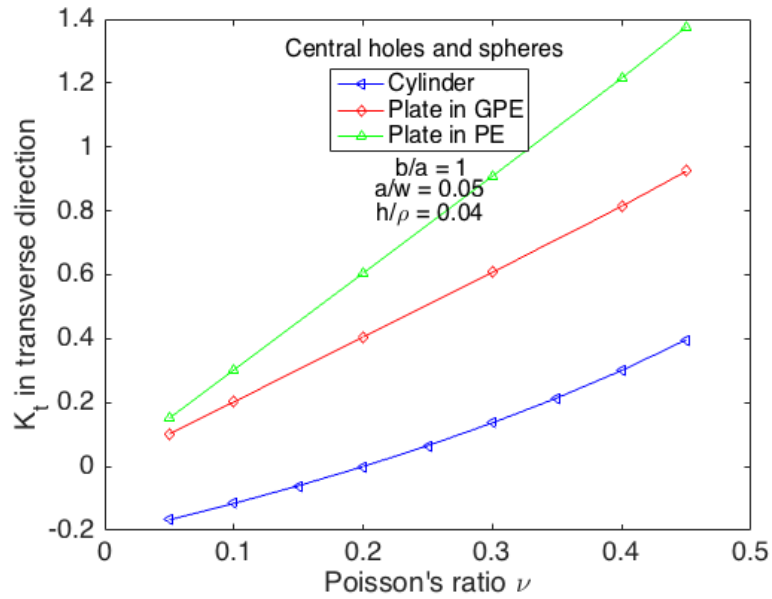
Central holes in plates and central spheres in cylinders have a considerable difference in constraints, and the same analogy as presented for grooves does not apply. Due to this, the SCF is lower at the notch root of a sphere than it is at the notch root of a circular hole. And the response to increasing Poisson's ratio is not expected to be equal. Even though the cross-section of a cylinder with a central sphere is a 2D plate with a circular hole, the constraints of these two models are different. The difference between the stress behaviour is directly visible when comparing Eq. (21) for a sphere and Eq. (16) for a plate with central hole in GPE.

Figure 20b shows the difference in transverse stresses between a cylinder with central sphere and a plate with a central hole, both when the plate is in GPE and PE. Both the cylinder and the plate in GPE responds similarly to increasing Poisson's ratio, but the solutions are quite different, as explained by the analytical equations.

Based on the analogy that the transverse SCF for thick plates with side-grooves and cylinders with circumferential grooves should be similar, the results show that plates in GPE give the most realistic real-life results from 2D plates.



(a) Cylinders with circumferential grooves and plates with side-grooves in PE and GPE.



(b) Cylinders with central spheres and plates with central holes.

Figure 20: The results from FEA for  $K_{tz}$  with changing Poisson's ratio for cylinders and plates in PE and GPE.





## 4 3D FEA of plates with central holes

The results presented so far, were all based on 2D FEA and solutions from the literature. This has provided a solid overview of the expected behaviour, both from the SCF and the stress gradient, for varying notch-shapes. Most importantly, the requirements for accurate FE-results were established from 2D FEA. These results are crucial for critical compilation of 3D stress data.

The following 3D study will focus only on central holes in plates, as this will allow for a deeper investigation of all affecting parameters. The study focuses on the effect of Poisson's ratio and thickness, as these properties are highlighted in recent papers [7]–[9]. The effect of these properties on the stress gradient is yet unknown, but is thoroughly studied here.

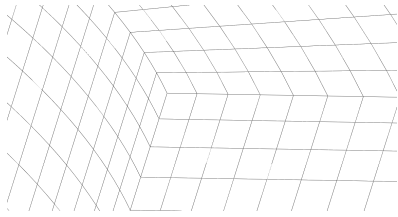
### 4.1 3D modelling technique

A 3D FE-model is made by a similar procedure as presented for 2D models, where the main difference is that the actual thickness of the plate is modelled. For 2D plates, only a quarter of the plate was needed for analyses, due to symmetry. By adding the additional symmetry through the half-thickness for 3D plates, only 1/8 of the plate is needed for FEA. The main incentive for utilising symmetry is to reduce computation time, and the computation time is highly challenged when running 3D FE-models.

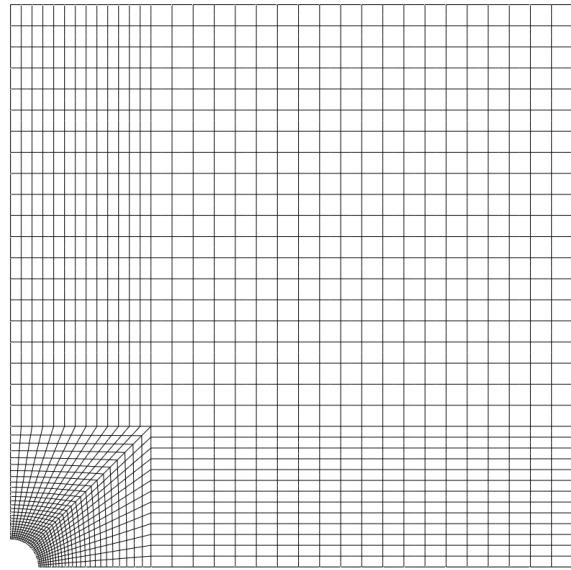
Meshing of the 3D model is also very similar to the 2D model, but 2D elements and 3D elements have some differences. The main difference is that 3D elements have three degrees of freedom at every node, while 2D elements have two. 2D elements have 4-8 nodes, all in the same plane, while the 3D elements have 8-20 nodes in three different planes. These are the main reasons why 3D calculations take much longer time to solve.

The desired mesh properties for 2D models were found from the 2D preliminary study, which resulted in satisfying accuracy. The same mesh can be used in 3D, but additional meshing is needed through the thickness of the plate. Figure 21 shows the mesh used for 3D FEA. The maximum SCF is expected to move towards the free surface of the plate with increasing plate-thickness [7]–[9], and the mesh density is highest in this region to accommodate for this. In Figure 21a is seen that the mesh density gradually increases towards the free surface, reducing the number of elements needed and hence the calculation time [15].

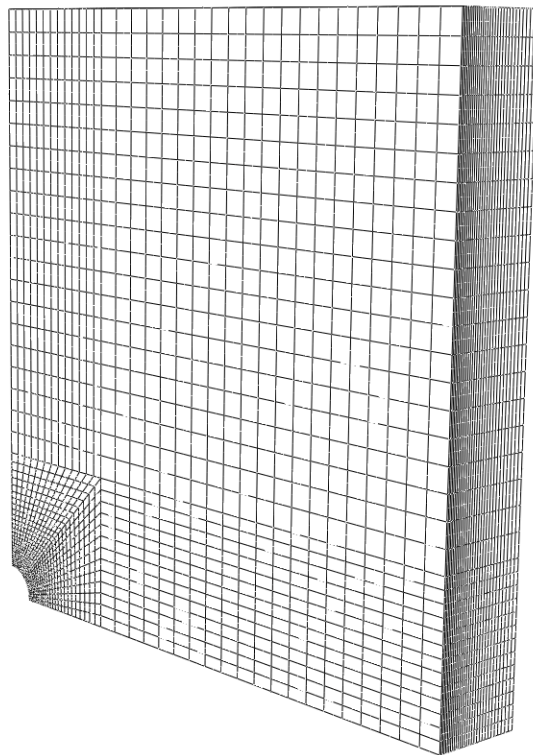
Elements with straight perpendicular edges give highest accuracy [13]. Thus, perfectly cubic elements are used at the notch root, at the free-surface, see Figure 21a. This means that moving from the mid-plane towards the free surface, the elements at the notch root become more like a perfect cube. The length of the cubic element is given by  $h/\rho = 0.06$  for all 3D models, as found from the prelimin-



(a) Mesh at the notch root



(b) Mesh at the free-surface, the same as in 2D



(c) Perspective view of the 3D mesh

Figure 21: 3D FE-mesh for a plate with a central circular hole

ary study. The actual number of elements and total degrees of freedom is different for every 3D model, increasing with increasing thickness and for decreasing radius of curvature  $\rho$ .

She and Guo [7] showed that the ratio of largest-to-smallest elements in the thickness direction affects the SCF results. They showed that it affected the SCF at the free-surface ( $K_{t,\text{surf}}$ ) the most, while the maximum SCF ( $K_{t,\text{max}}$ ), and the overall stress concentration through the thickness, remained rather stable. Thus this is not a concern, as the main focus is on the behaviour of the maximum SCF. However, all 3D FE-models used are well within the convergent largest-to-smallest element ratio, without a specific statement.

By applying the same mesh as in 2D, to the 3D models, it reduces the need for a 3D preliminary study, saving time. As there are no analytical 3D solutions to compare with, the preliminary 2D results are actually the only reliable results to base further 2D and 3D analyses on. The final accuracy of the 3D model can be controlled by a 3D PE analysis, as will be presented in the following.

## 4.2 Plane strain solution

Through extensive work with thin plates, a good resemblance between analytical solutions and the FE-results was assured. This indicated that the FE-models that were used, gave theoretically accurate results for thin plates. It is assumed that the accuracy remains when transitioning from 2D FEA to 3D FEA, however this is not yet tested. To verify the actual accuracy, the FE-results for 2D plates can be compared to FE-results for 3D plates in PE. This is possible because  $\sigma_y$  at the notch root should be equal for plates in PS and PE. The PE condition for a 3D model can be found by restricting the displacement in  $z$ -direction, as suggested by She and Guo [7]. This method is used as a tool to further control the accuracy of the FE-models, assuring that the accuracy is maintained when transitioning from 2D FEA to 3D FEA.

The results from 3D FEA in PE for various central notches are presented in Table 4, and the corresponding results from 2D FEA are also provided, for comparison. The deviation between these results can be calculated from

$$\% \text{ Error} = 100 \times \left( \frac{K_{t,3D}}{K_{t,2D}} - 1 \right) \quad (23)$$

which gives the percent error of the 3D model relative to the 2D model.

Table 4 shows that the 3D models deviate by 0.07%–0.1% from the 2D results, for the notch shapes that were studied. From the preliminary study it is also known that the accuracy of the 2D model is high, with a maximum deviation of 0.1% from the estimated theoretical solution  $K_{t,(h=0)}$ . Ultimately, the 3D FE-results for PE

Table 4: Results from 2D FEA and 3D FEA in PE, where  $a/w = 0.05$  and  $h/\rho = 0.06$  for all models.

Results from FEA	b/a = 0.5	b/a = 1	b/a = 2
$K_t$ 2D plane stress	5.0303	3.0242	2.0249
$K_t$ 3D plane strain	5.0338	3.0268	2.026966
% Error in 3D	0.07%	0.09%	0.1%

are extremely accurate, providing good grounds for reliable 3D SCFs and stress gradients. As a prerequisite for fatigue life calculations, it was desired that the 3D FE-results had errors less than 1%. The results show much higher accuracy than this, even without introducing extreme mesh requirements. In comparison, She and Guo [7] states that their models were within 0.7% error in all cases that they studied. Thus the accuracy of the 3D FEA that is used here is considerably higher than what has been used in previous research.

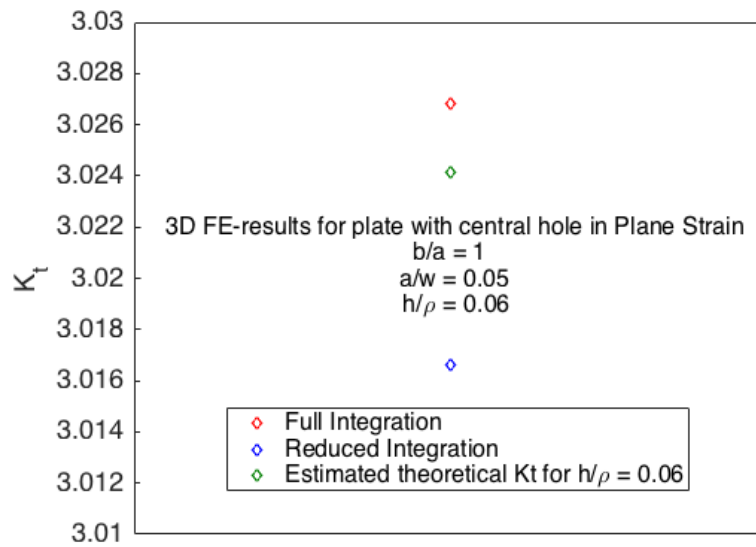
The PE analysis can also be used to check the difference in accuracy between full integration and reduced integration, where full integration was used in the results presented above. Figure 22 shows the SCF results for both full integration and reduced integration, where it is seen that full integration gives an overestimate of  $K_t$  relative to the estimated theoretical solution for  $h/\rho = 0.06$  (from Figure 7, Section 2.1.4). Reduced integration gives an underestimate of the theoretical  $K_t$ -value for  $h/\rho = 0.06$ .

Figure 22a shows the results for a circular hole, while Figure 22b shows the results for an ellipse where  $b/a = 0.5$ . For an elliptic hole, both the solutions for full and reduced integration are further away from the estimated theoretical solution than for a circular hole. It is reasonable that such effects increase with increasing SCF. However, the difference between full integration and reduced integration, relative to the theoretical solution, seems to be consistent between the figures.

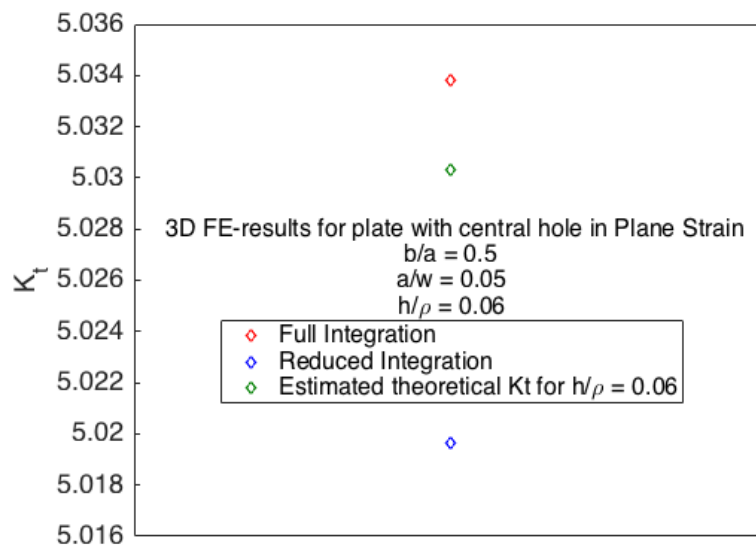
Even though the accuracies found in Table 4 are from 3D FEA using full integration, the accuracies when using reduced integration are also great. The results presented in Figure 22a and Figure 22b show errors of only 0.26% and 0.21%, respectively, for reduced integration. Based on this, both full and reduced integration can be chosen with confidence for the models studied. As will be shown in the next section, only reduced integration was achievable.

### 4.3 The 3D stress distribution

The stress distribution ahead of a thin plate is two-dimensional, as a thin plate is in PS which requires that  $\sigma_z = 0$  everywhere. Figure 23 shows the typical stress distribution from 2D FEA, ahead of different central elliptic holes. The stress acting in  $x$ -direction is always zero at the notch root, as it acts perpendicular to



(a) Plate with central circular hole in PE.



(b) Plate with central elliptic hole in PE.

Figure 22: SCF for plates in PE with central a) circular holes and b) elliptic holes, comparing the effect of full and reduced integration. The results are compared with the estimated theoretical result when  $h/\rho = 0.06$ .

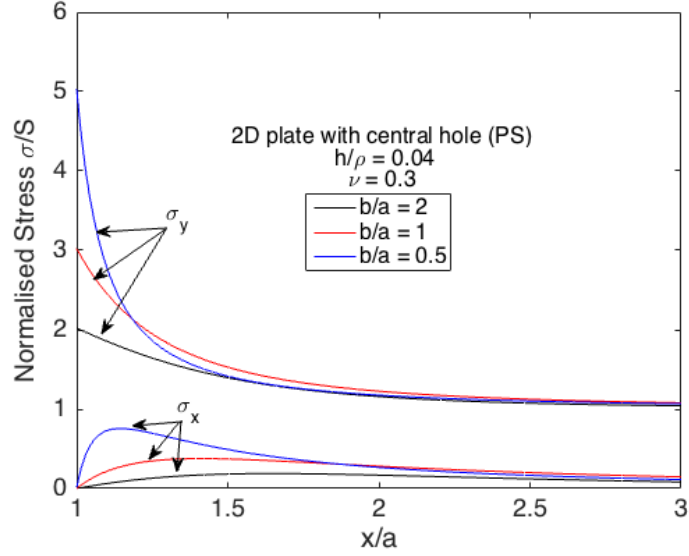
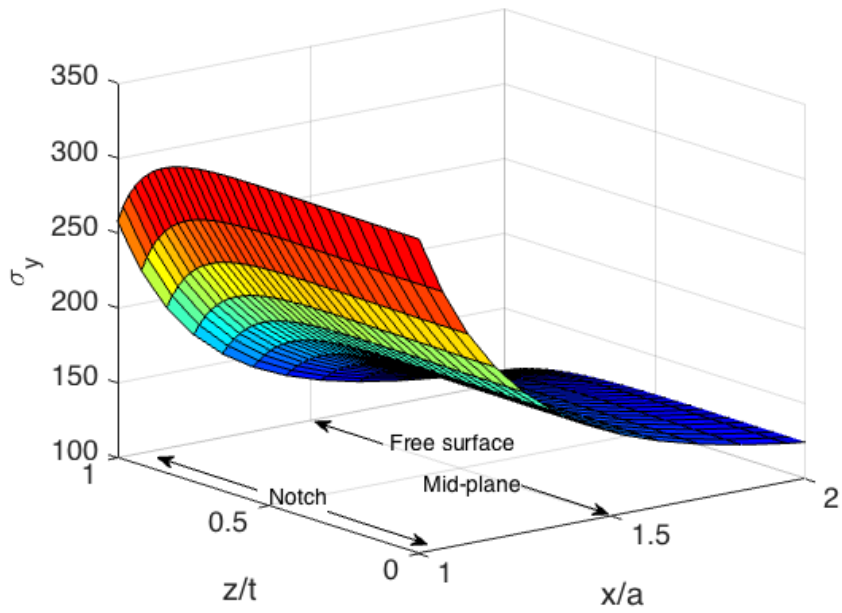


Figure 23: The stress distribution ahead of a central notch in a 2D plate, showing the 2D FE-results for both elliptic and circular holes.

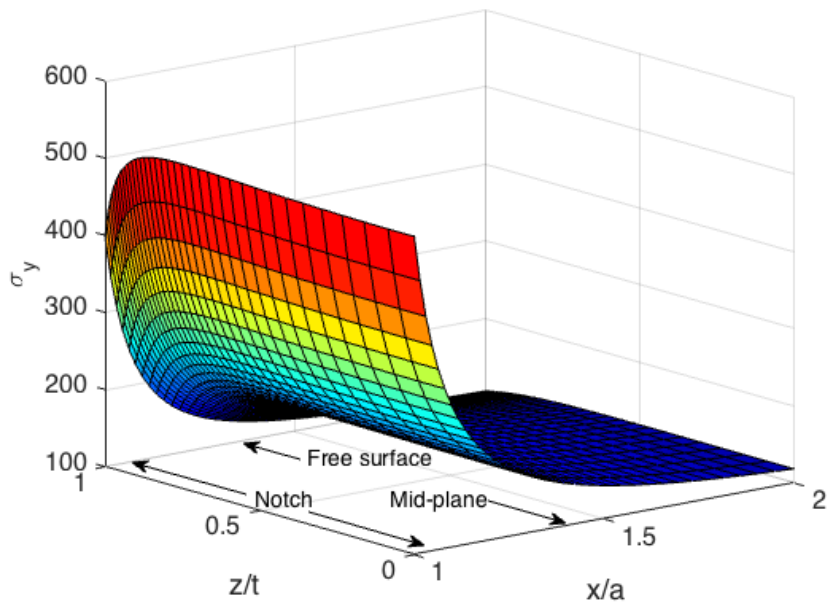
the free surface. The stress in  $y$ -direction has its maximum at the notch root, and decreases towards the value of the applied stress far away from the notch. The maximum stresses seen in Figure 23 are consistent with Inglis' equation, Eq. (4), where the maximum stress increases as  $b/a$  decreases. The stress distribution for an ellipse with  $b/a = 2$  is very moderate compared to the others, and the main focus for the 3D study of plates will be on holes where  $b/a = 0.5$  and 1, as they cause higher stress concentrations.

If considering the axial stress,  $\sigma_y$ , it is possible to grasp the extent of the 2D behaviour, while trying to imagine how  $\sigma_y$  changes through the thickness of a 3D plate becomes complicated. Figure 24 shows the actual stress distribution of  $\sigma_y$  through the thickness of a plate, in the region close to the notch, as found from 3D FEA with  $t/a = 3$ . Figure 24a shows the results for a central circular hole and Figure 24b shows the results for a central elliptical hole with  $b/a = 0.5$ . A more dramatic stress distribution is observed for the ellipse than for the circle.

Figure 24 confirms that  $\sigma_y$  changes through the thickness of the plate, and the effect of thickness and the Poisson's ratio on  $K_t$  will be studied closely. For 3D structures,  $\sigma_x = 0$  at the notch root, but a stress  $\sigma_z$  is acting in the thickness-direction of the material. The behaviour of  $K_{tz}$  will thus also be studied thoroughly.



(a) Stress distribution  $\sigma_y$  ahead of a circular hole



(b) Stress distribution  $\sigma_y$  ahead of an elliptic hole ( $b/a = 0.5$ )

Figure 24: The 3D stress distribution of  $\sigma_y$  ahead of a central a) circular hole and b) elliptic hole from 3D FEA.

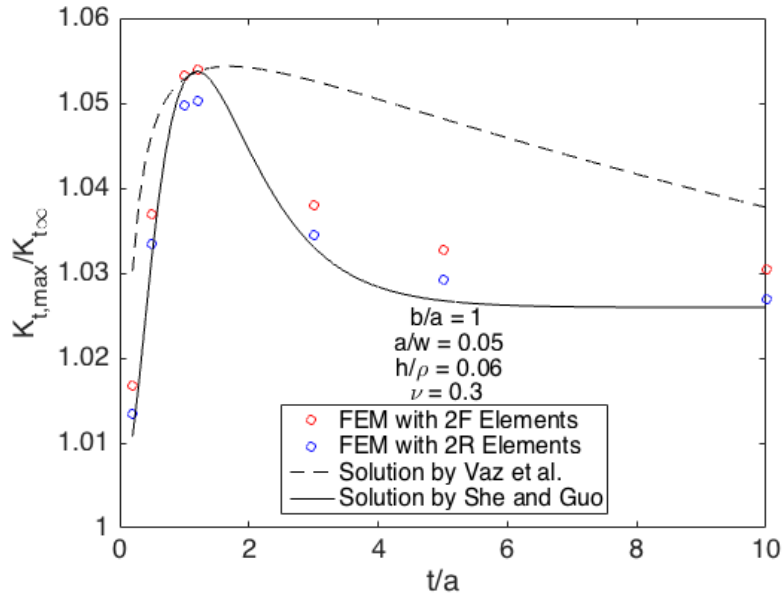


Figure 25: Maximum SCF from FEA with increasing plate thickness, for both full and reduced integration. Equations from recent papers [7], [9] are also presented.

#### 4.4 The effect of thickness

Apart from the analytical solutions for plates in PS and PE, the stress distribution ahead of notches of any real plate thickness is unknown, or at least not fully established and accepted. 3D FEA makes it possible to study the stress behaviour in plates of any plate thickness, and the preliminary study shows that it is a reliable tool.

##### 4.4.1 The effect of thickness on the stress concentration factor

She and Guo [7] and Vaz et al. [9] both have developed equations to approximate the effect of thickness on the maximum SCF. The maximum SCF at circular holes, found from 3D FEA for many plate thicknesses, is compared to these equations in Figure 25. The FE-results are here normalised by the analytical solution  $K_{t\infty} = 3$ , as this is the approach used in the papers [7], [9]. Both the FE-results and the equation by She and Guo are specific for  $a/w = 0.05$ , while the equation by Vaz et al. is valid for all ratios. The effect of finite width is low when  $a/w = 0.05$ , the equation by Vaz et al. becomes inaccurate for this specific case. With increasing thickness, the SCF is expected to reach a constant value as it reaches GPE, which is not the case with Vaz et al.'s solution in Figure 25.

A small difference between She and Guo's results and the FE-results is also



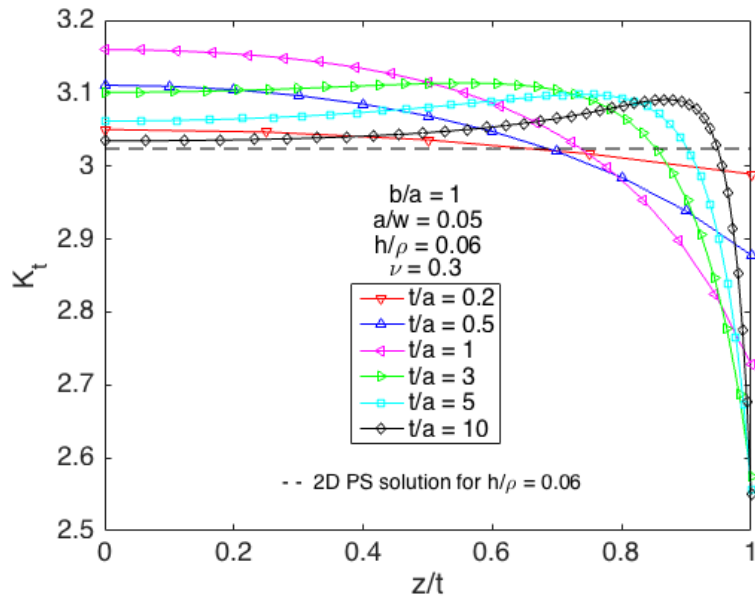
noticed in Figure 25. First of all, there is a difference in accuracy between these two studies. The PE test showed that the results from FEA have a maximum error of 0.07%, while She and Guo states that their PE test gave a maximum error of 0.7% for their FE models. Also, it is seen from the plot presented by She and Guo [7], that their numerical results for this specific case lie above the equation for large  $t/a$ . This means that the FE-results from both these studies are more alike than it seems from Figure 25. Ultimately, She and Guo's formula is a general equation that can be applied to any elliptical shape, which means that it cannot be expected that this equation is in exact agreement with the FE results that are specific for  $b/a = 1$ .

A comparison between full and reduced integration (2F and 2R respectively) is also found in Figure 25. For the plate thicknesses that cause the largest SCFs, it is seen that reduced integration gives an underestimate of the maximum value. If extrapolating the curves in Figure 25 to  $t = 0$ , the solution for full integration ends up at 1, while reduced integration ends up below. From this, it seems like full integration is the most conservative choice for the specific cases studied here. Figure 25 also shows that the 2R and 2F solutions have a very consistent difference of approximately 0.4%. So the same conclusion is reached as from the PE test of the 3D model; the accuracy using both full and reduced integration is more than satisfying for the purpose of this research.

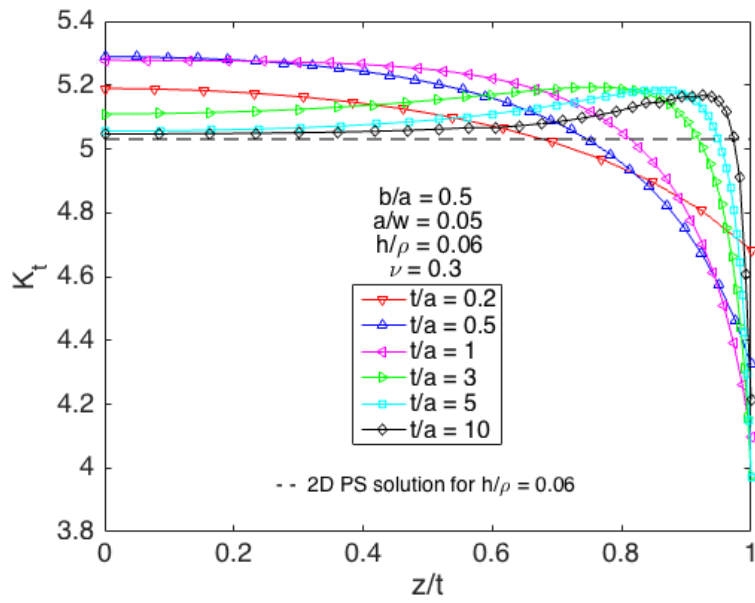
Full integration is favourable because it gives a maximum SCF value that corresponds to the results from both [7], [9], but it is also the most computationally expensive choice. As it is very difficult to solve 3D FEA for elliptical holes with  $h/\rho = 0.06$  using 2F elements, 2R elements will be used so that the accuracy related to  $h/\rho = 0.06$  is maintained throughout this thesis.

Figure 25 shows that the value of the maximum SCF changes with increasing thickness. The general stress distribution through the thickness of the plate changes with increasing thickness as well. This non-uniform stress distribution is highlighted in recent research [7]–[9], [18]. Figure 26 shows the changes in SCF, through the thickness of plates with various plate thicknesses, found from 3D FEA. Both the results caused by a central circular hole and a central ellipse with  $b/a = 0.5$  are shown, and the estimated theoretical solution for  $h/\rho = 0.06$  (see Figure 7) is plotted for comparison.

It is very clear from Figure 26 that the SCFs inside the material are much higher than those at the free surface of the plate. If the SCFs at the mid-plane are considered, it is observed that thin plates lie close to the 2D PS solution and with increasing thickness the SCF increases drastically. Eventually, before the plate thickness reaches  $t/a = 3$ , the SCF decreases again. The solution approaches a PE solution with increasing thickness, essentially the 2D PS solution. This trend was also seen from maximum SCF behaviour in Figure 25. Figure 26b shows that



(a) Plate with central circular hole



(b) Plate with central elliptic hole

Figure 26: Change in SCF through the thickness of plates with a central a) circular hole and b) elliptic hole. The FE-results for various plate thicknesses are presented together with the 2D solution found in Table 4.

the behaviour is more dramatic for the ellipse, as the SCF is higher directly causing out-of-plane stresses to appear for thinner plates.

If studying the behaviour of the maximum SCF in Figure 26, the maximum is found at the mid-plane for thin plates, and moves away from the mid-plane towards the free-surface of the plate with increasing plate thickness. Vaz et al. [9] found that for thicknesses  $t/a \leq 1.5$  the maximum SCF remains at the mid-plane of the plate. However, when the thickness is above  $t/a = 1.5$ , they showed that the location of  $K_{t,\max}$  moves away from the mid-plane and towards the free-surface of the plate, but it never reaches it. This corresponds well with the observations from Figure 26.

The position  $z_{\max}$  of maximum SCF through the thickness of the plate, where  $K_t = K_{t,\max}$ , is presented in Figure 27. The position  $z_{\max}$  for all plate thicknesses studied by FEA are presented in the figure, for both plates with circular holes and elliptic holes. It is found from Figure 27 that  $z_{\max}$  is closer to the free-surface of the plate for the elliptical hole than for the circular hole. This gives reason to believe that that  $z_{\max}$  is closer to the free-surface of the plate for notches with lower notch root radii, which was also pointed out by She and Guo [7].

Figure 27 shows that when  $t/a \leq 1.2$ , the maximum SCF remains at the mid-plane for both circular holes and elliptical holes, which is also observed in Figure 26. This is confirmed by Vaz et al. [9]. Figure 27 confirms that the maximum SCF never reaches the free surface of the plate Vaz et al. [7], [9]. When graphically comparing the results from FEA of a plate with circular hole and the results presented by Vaz et al. [9], they seem satisfyingly similar. The exact numerical values are difficult to draw from the figure, but the results by Vaz et al. are expected to be less accurate, as they are based on FEA with first order elements, but such effects are not directly visible when comparing the graphs.

A conventional way to find the SCF for fatigue assessments is by measuring the stresses at the free-surface of the structure [7]. The results from FEA, as well as from previous research [7]–[9], show that the through-thickness maximum SCF is in fact not found at the free-surface of the plate. Thus, finding the difference between the SCF at the free-surface and at the actual maximum becomes relevant. Figure 28 presents the ratio of the maximum value and the surface value for varying plate thicknesses, as found from FEA. An increase in the maximum SCF relative to the surface value is seen for increasing thickness, until a critical thickness is reached, where  $K_{t,\max}/K_{t,\text{surf}}$  becomes constant due to GPE. The equation developed by She and Guo [7] is also plotted in Figure 28, which shows the exact same behaviour. She and Guo tested many elliptical shapes and concluded that  $K_{t,\max}/K_{t,\text{surf}}$  is elevated with decreasing radius of curvature at the notch root, confirming the trend seen in Figure 28.

Vaz et al. [9] found that the maximum SCF is 24% higher than the value at

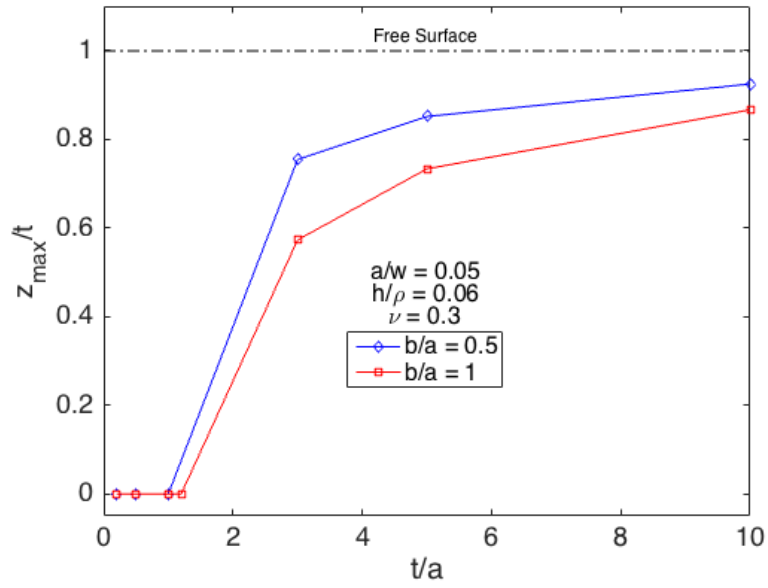


Figure 27: The location of  $K_{t,\max}$  inside the plate, given as the distance  $z_{\max}$  away from the mid-plane for different plate thicknesses.

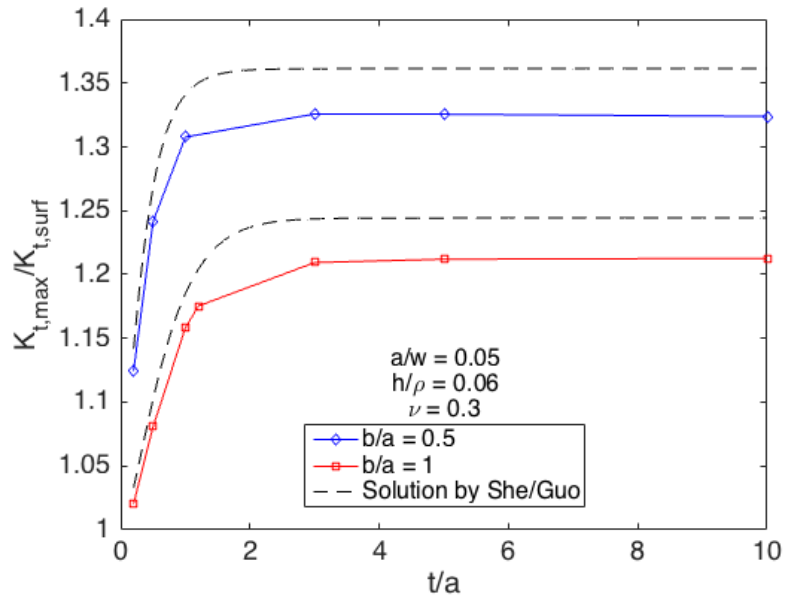


Figure 28: The change in the ratio of maximum SCF relative to the SCF at the free-surface of the plate, for increasing plate thickness.

the free-surface of a circular hole when  $t/a \geq 5$ . In Figure 28 the maximum value is 21.3% higher than the value at the free-surface for plates with circular holes and 33% higher for plates with elliptical holes. The overall SCF behaviour from FEA is consistent with the equation by She and Guo and the descriptions by Vaz et al..

#### 4.4.2 The effect of thickness on the transverse stress

The main difference between studying a 2D model and a 3D model of the same structure, is considering what happens through the thickness of the material. It was just shown how the stress in the longitudinal direction ( $\sigma_y$ ) changes through the thickness, but this is also directly related to the material behaviour in the transverse directions [20]. At the notch root,  $\sigma_x = 0$ , and thus only the stress in  $z$ -direction of the transverse plane is relevant. The PE condition assumes no strain through the thickness, but it has already been discussed that GPE is more realistic.

The transverse SCF acting in  $z$ -direction under GPE can be found by rewriting Eq.(16), which gives:

$$K_{tz} = \nu(K_t - 1) \quad (24)$$

where  $K_t$  is the SCF in  $y$ -direction.

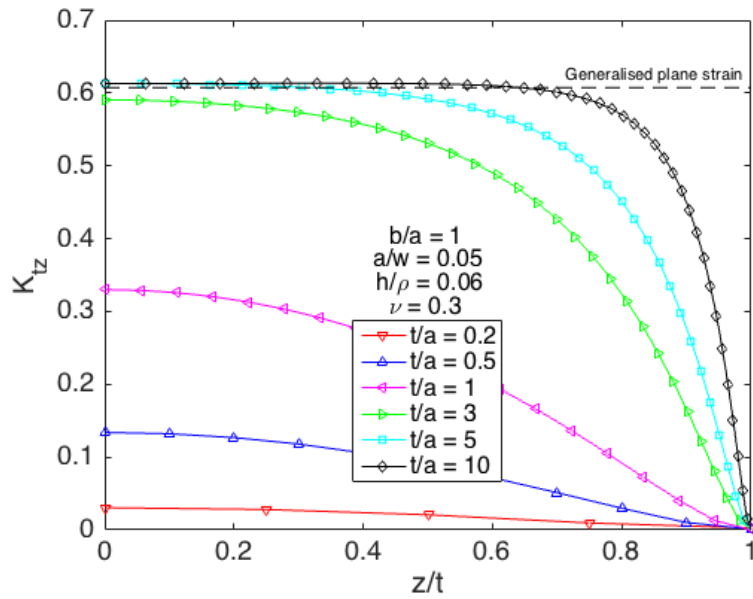
Eq.(24) can be used together with the FE results, to evaluate the state of the material. Figure 29 presents the FE-results for the SCF in  $z$ -direction, for plates with central circular holes and elliptic holes. The figure includes the FE results for all plate thicknesses studied, however the solution for  $t/a = 10$  is removed from Figure 29b, as it gives almost the exact same result as for  $t/a = 5$ .

Eq.(24) is plotted in both figures, so that the GPE condition inside the material can be observed. The plate cannot have GPE everywhere, as  $\sigma_z$  must be zero at the free-surface, which means PS. This is why a sudden decrease in  $K_{tz}$  is observed close to the free-surface in Figure 29. The transverse stress appears as a reaction to the material that tries to contract more in the region close to the notch, where stresses are higher than in the surrounding material. As the SCF is higher for an ellipse, Figure 29b reaches GPE for lower thicknesses than the circular hole in Figure 29a, as also observed in Figure 26.

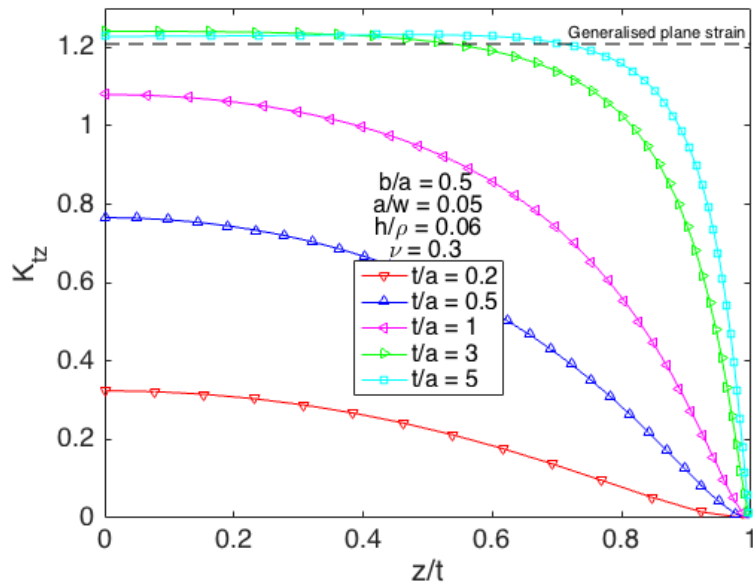
The constant strain inside the material that reaches GPE can be calculated. Hooke's law for  $\varepsilon_z$  was expressed in Eq.(12). At the notch root,  $\sigma_y = K_t S$  and  $\sigma_x = 0$ , and the equation for transverse strain at the notch root can be written as

$$\varepsilon_z = \frac{\sigma_z}{E} - \nu \frac{K_t S}{E} \quad (25)$$

where the results found in Figure 29 can be used to calculate the constant strain.



(a) Plate with central circular hole



(b) Plate with central elliptic hole

Figure 29: The change in  $K_{tz}$  through the thickness of the plate for various plate thicknesses. The results are compared with the solution from Eq. (24) for GPE.

Figure 29 showed that  $\sigma_z$  was constant and equal to the GPE solution inside the material for the largest plate thicknesses studied. The equation for  $\sigma_z$  in GPE is known, see Eq.(16), and can be inserted into Eq.(25) which gives

$$\varepsilon_z = \nu \frac{(K_t - 1)S}{E} - \nu \frac{K_t S}{E} = -\nu \frac{S}{E} = -0.3 \times \frac{100}{200000} = -1.5 \times 10^{-4}$$

when the Poisson's ratio  $\nu = 0.3$  and Young's modulus  $E = 200.000$  MPa.

Thus, the strain through the thickness of the structure, in the regions with GPE, is equal to  $-1.5 \times 10^{-4}$  for the FEA case shown in Figure 29. The same equation can be used to calculate the strain in the region of GPE for any other applied stress, Young's modulus and Poisson's ratio.

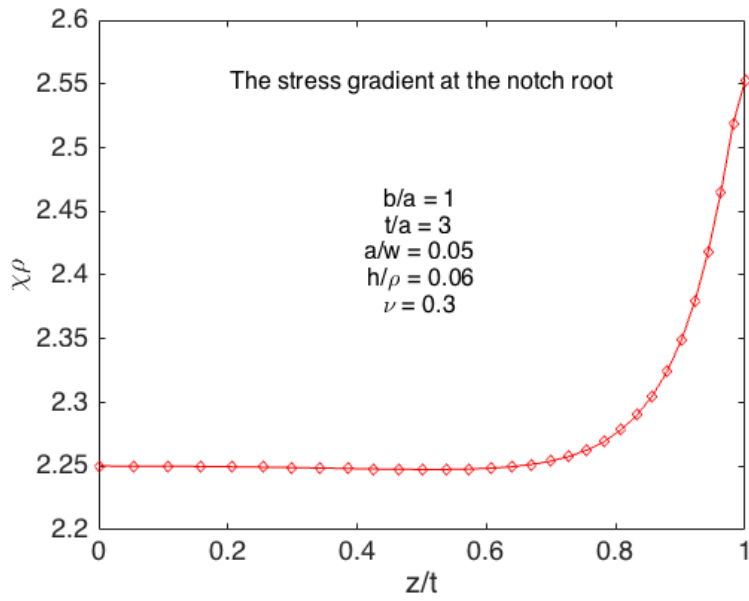
#### 4.4.3 The effect of thickness on the stress gradient

The changes in SCF through the thickness of the plate was further enhanced by increasing thickness, and it is expected that the stress gradient reflects a similar behaviour. The relative stress gradient can be calculated from Eq.(6), which is directly related to the SCF. The analytical solution for the stress gradient was  $\chi\rho = 7/3$  for a circular hole and  $\chi\rho = 11/5$  for an elliptic hole. However, as  $h/\rho = 0.06$  for 3D FEA, the FE-results are not expected to reach the analytical solution, but the estimated theoretical solution for  $a/w = 0.05$  and  $h/\rho = 0.06$ . As found from Figure 12, the estimated theoretical solution is  $\chi\rho = 2.265$  for circular holes and  $\chi\rho = 2.125$  for elliptic holes. With the use of these values, any numerical errors from FEM are accounted for.

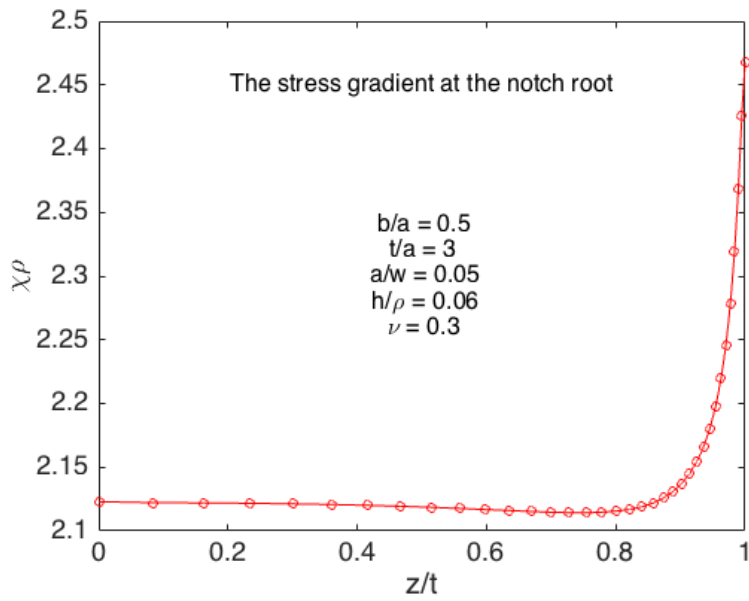
By utilising the method developed in the preliminary study, the stress data from FEA was used to calculate  $\chi\rho$  at every point through the thickness of plates with thickness  $t/a = 3$ . This procedure was performed for both circular holes and elliptic holes. In Figure 30 the results are presented, and it is clear that  $\chi\rho$  is much higher at the free surface of the plate than anywhere else within the material. At the same time, the lowest stress gradient is found inside the material. In fact, the lowest  $\chi\rho$  inside the plate is 0.8% – 0.94% below the estimated theoretical solution, for both elliptical and circular holes.

As the results in Figure 30 are for one specific plate thickness, it is not enough to make a general statement. Figure 31 presents  $\chi\rho$  for all plate thicknesses studied by FEA. Three curves are plotted, representing the stress gradients found at the mid-plane, at the free surface and at the point where  $K_t = K_{t,\max}$ . The behaviour from Figure 31 is consistent for all plate thicknesses studied. The highest stress gradient is found at the free surface of plates, while the lowest stress gradient is always where  $K_t = K_{t,\max}$ .

It was previously shown (in Figures 26 and 29) that for small thicknesses,  $K_{t,\max}$  remains at the mid-plane. This is why the stress gradients at the mid plane



(a) Plate with a central circular hole



(b) Plate with a central elliptic hole

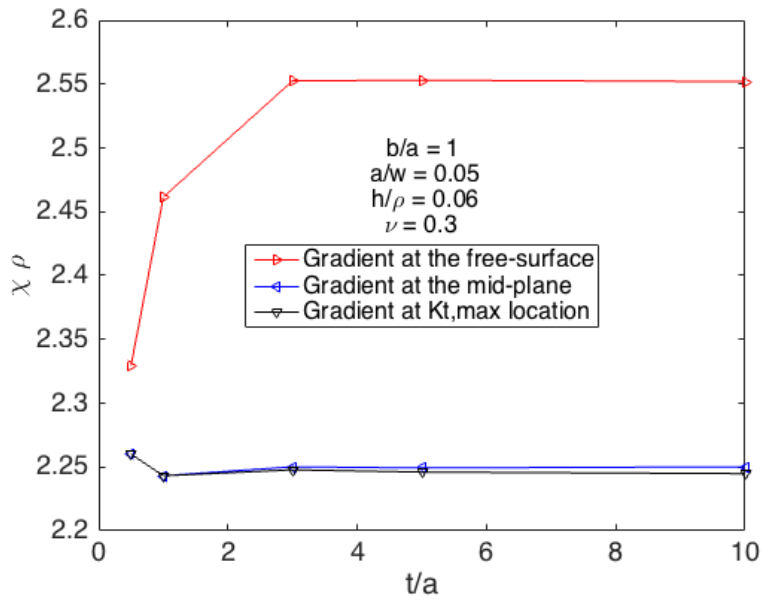
Figure 30: The stress gradients through the thickness of the plate, along the notch from the mid-plane towards the free surface, for a plate with half-thickness  $t/a = 3$ .



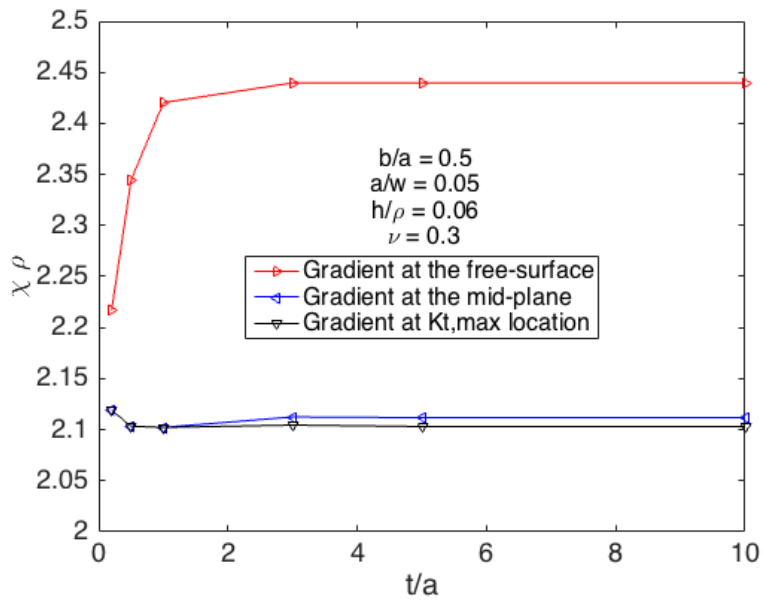
and at  $K_{t,\max}$  are equal for small plate thicknesses. It observed that the stress gradients found at the mid-plane and at  $K_{t,\max}$  are very similar even for larger plate thicknesses. This was also observed from Figure 30.

The FEA results also clearly indicate that the stress gradient at the free-surface of the plate is much higher than the estimated theoretical solution, for all plate thicknesses studied. For  $t/a \geq 3$ , the stress gradient at the free surface is approximately constant, 12.7% and 14.8% higher than the estimated theoretical solution for the circle and ellipse respectively.

The most important finding from Figure 31 is that the point of  $K_{t,\max}$  always has the lowest stress gradient. Schijve [14] stated that a steep gradient was more favourable than a low gradient. He explains that the volume of highly stressed material is larger when the stress gradient is low. For 3D plates with central circular holes and elliptical holes, the lowest stress gradient is lower than the analytical value, where  $K_{t,\max}$  is higher than the analytical value at the same time. This means that the volume of highly stressed material is much larger in this region than anticipated from theory. It is unknown how much a 1% decrease in stress gradient, relative to the estimated theoretical value, means for fatigue life. A simple fatigue life assessment will be presented in Section 5, to show the relation between the different impacting factors, and how the findings may affect the fatigue calculations.



(a) Plate with central circular hole



(b) Plate with central elliptic hole

Figure 31: The variation of the stress gradient  $\chi\rho$  with increasing thickness. The value found at the free surface of the plate, at the mid-plane and at the location of maximum SCF are compared for a plate with a central hole.

## 4.5 The effect of Poisson's ratio

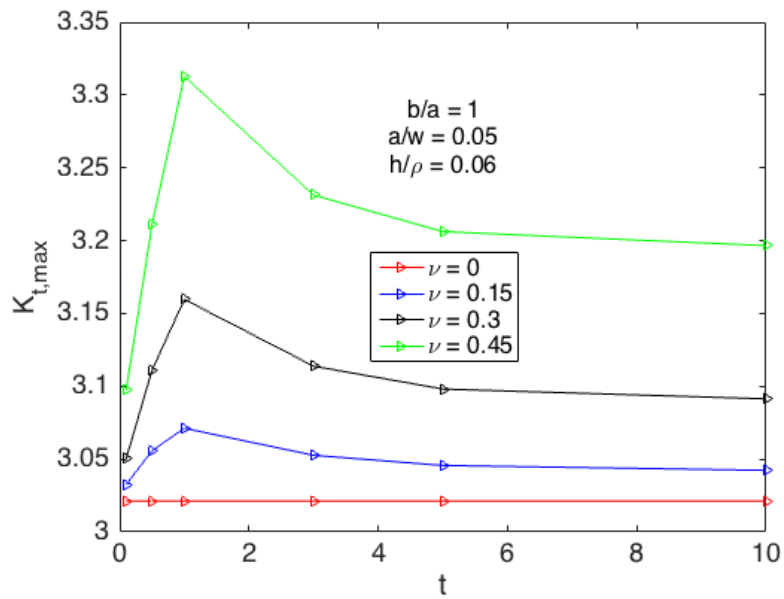
One of the main benefits of analysing structures by FEM is that any parameter is easily changed. Not only does this involve the geometrical parameters, but also material constants, such as the Poisson's ratio. Already, the relationship between the applied stress in the longitudinal direction and the transverse response has been studied. The Poisson's ratio is an essential part of Hooke's law, and in the following the actual effect it has on the SCF and stress gradient will be studied closely. If the effect of Poisson's ratio is known, it becomes possible to predict the changes in SCF between different materials.

### 4.5.1 The effect of Poisson's ratio on the stress concentration factor

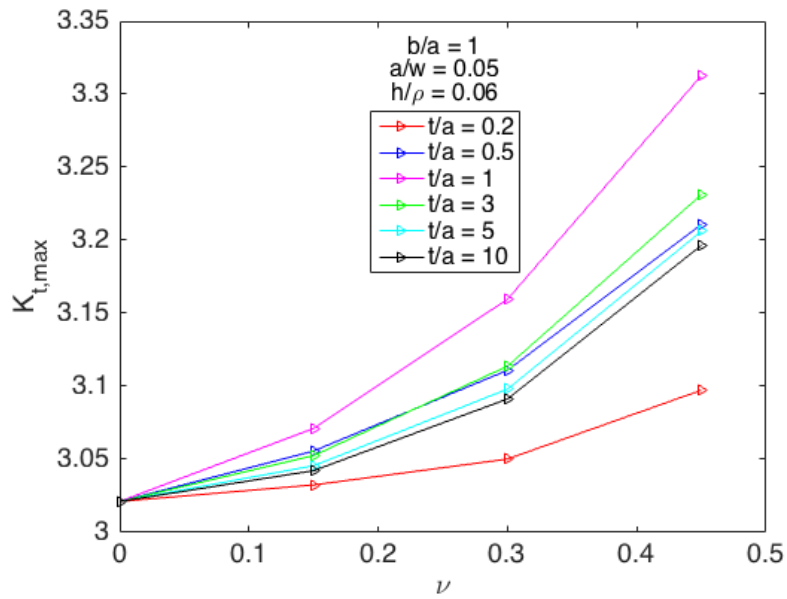
The Poisson's ratio of the material controls the transverse contraction of the structure, and when a plate is loaded in uni-axial tension, contractions in both the width- and thickness directions are expected for most materials. The stress at the notch root is much higher than everywhere else in the material, causing the material close to the notch root to contract more in the thickness direction than the surrounding material with lower stresses [2], [21]. This causes a constraint in the thickness direction, and due to mechanical equilibrium, a stress in the thickness direction of the material ( $\sigma_z$ ) appears. By Hooke's law, this stress depends on the Poisson's ratio, and it becomes reasonable to question how this affects the maximum SCF at the notch root.

In a recent paper by Yu et al. [8] the relation between SCFs and the Poisson's ratio was carefully studied for many elliptical shapes, plate thicknesses and Poisson's ratios. The following is an approach that serves the purpose of supporting their results by controlling their solution, as well as connecting the results to the behaviour of the stress gradient. Yu et al. showed that increasing the Poisson's ratio directly leads to an increase in the maximum SCF. They found that when the Poisson's ratio goes from  $\nu = 0.1 - 0.49$ , the peak value of  $K_{t,\max}$  increases by 9% for a plate with a circular hole. The results from 3D FEA of a plate with central circular hole for varying thickness and Poisson's ratio is shown in Figure 32a, which is similar to the figure provided by Yu et al. [8]. Unfortunately an error was discovered in the equation developed by Yu et al. and because of this, their solution was not plotted in Figure 32a. The peak value of  $K_{t,\max}$  in Figure 32a increases by 9.65% when  $\nu = 0 - \nu = 0.45$ . This result confirms the solution found by Yu et al. [8]. Yu et al. also showed that the peak value of  $K_{t,\max}$  for increasing thickness is found when  $1 \geq t/\rho \leq 1.5$  for all elliptic shapes, which is also the case in Figure 32a.

Another way to present the result is by plotting the  $K_{t,\max}$  results for varying Poisson's ratio with each thickness separately, as shown in Figure 32b. Here the



(a) Maximum SCF when thickness is varied.



(b) Maximum SCF when Poisson's ratio is varied.

Figure 32: Maximum SCF from FEA of 3D plates with central circular holes with varying thickness and Poisson's ratio.

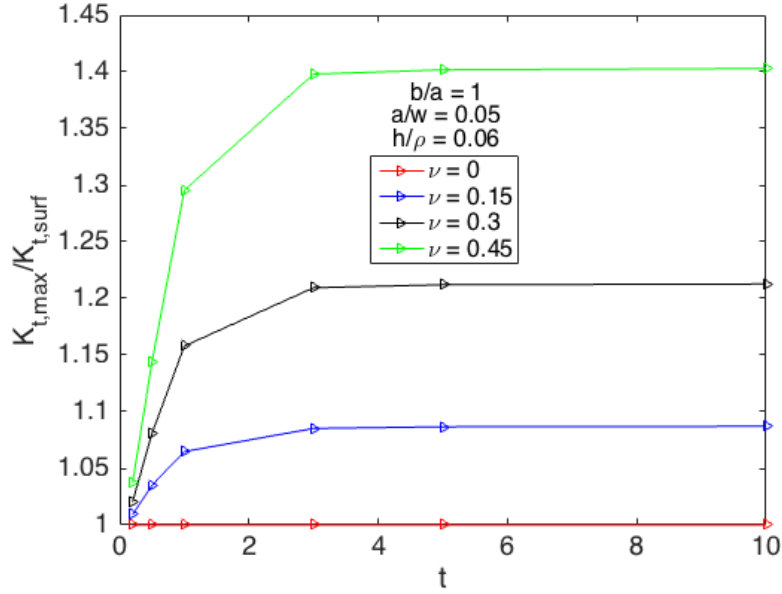


Figure 33: The ratio of maximum SCF and the SCF at the free surface for increasing thickness and varying Poisson's ratio.

effect of increasing Poisson's ratio is clearer, where the increase in  $K_{t,max}$  with increasing Poisson's ratio is consistent for any plate thickness. Yu et al. [8] found the same behaviour for all elliptic geometries that they studied,  $0.1 \geq b/a \leq 1$ .

It might also be noticed from Figure 32b that all plate thicknesses give the same  $K_{t,max}$  when  $\nu = 0$ . The value at this point is  $K_{t,max} = 3.0212$ , the same value as the estimated theoretical result for  $h = 0$ . The value at  $h = 0$  was found from extrapolation with the assumption of a theoretically perfect mesh. The reason why this value appears in Figure 32b is that when  $\nu = 0$  there will be no transverse material contraction, only longitudinal stress and strain. Thus, the element length  $h$  remains unchanged in the  $x$ -direction, meaning that the mesh refinement at the notch root has no effect on the solution. This result actually confirms the assumption from the preliminary study, that  $K_t = 3.0212$  is a good approximation of the analytical solution for a finite-width plate where  $a/w = 0.05$ .

Figure 33 shows that  $K_{t,max}/K_{t,surf}$  also changes with Poisson's ratio. Previously, when studying the effect of thickness, it was mentioned that the maximum SCF becomes 21.3% higher than the value at the free surface. This was when  $\nu = 0.3$  and in Figure 33 the same value is found. For  $\nu = 0.45$ , that the maximum SCF becomes 40% higher than the value at the free surface, confirmed by Yu et al. [8] who got 38%. This means that measuring the SCF at the free surface always leads to an unrealistic overestimate of the fatigue life.

### 4.5.2 The effect of Poisson's ratio on the transverse stress

The effect of Poisson's ratio on the transverse SCF in  $z$ -direction is shown in Figure 34 for a central hole with varying plate thickness. In Figure 34a the lines for GPE are also plotted, and it is seen that a GPE condition is reached for large thicknesses when  $\nu \geq 0$ . From Eq.(24) it is found that for  $\nu = 0.15, 0.3$  and  $0.45$ , the  $K_{tz}$  for GPE is  $0.303, 0.606$  and  $0.909$ , respectively. When  $\nu = 0.45$ , the transverse contraction is so large that the actual  $K_{tz}$  reached for GPE is higher than the one estimated from Eq.(24). For  $\nu = 0$  the transverse stresses are zero and the structure is left with only longitudinal stress and strain, according to Hooke's law [2].

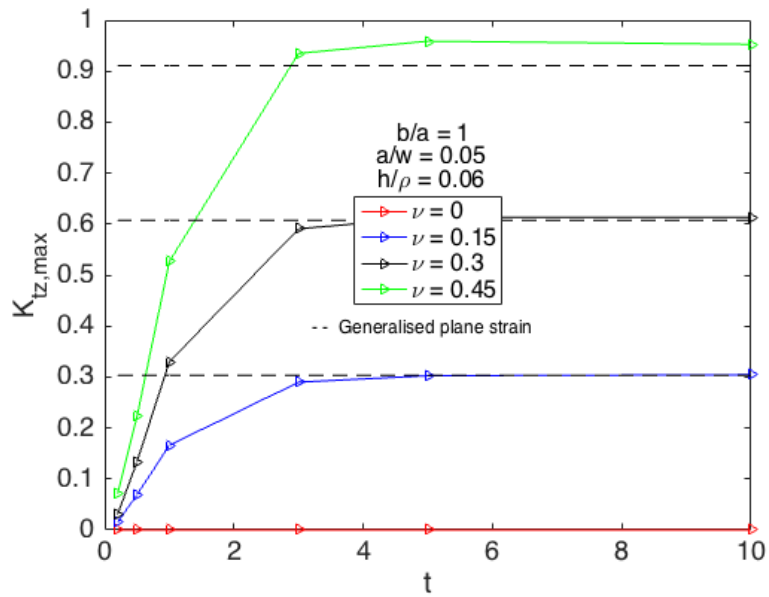
Figure 34b shows how each of the plate thicknesses vary with Poisson's ratio. The results for every thickness with increasing Poisson's ratio seem consistent, as all functions are approximately linear. Because the linear curves remain linear when they reach  $\nu = 0.45$ , it is reasonable that the effect of the Poisson's ratio, as explained above, is what causes the elevated GPE value for  $\nu = 0.45$  in Figure 34a.

The results in Figure 34b can be compared to the results found in the 2D study of plates in GPE. If considering the trend in Figure 34b it looks like the solutions for largest thicknesses converge towards the same solution, and these solutions remain equal for all Poisson's ratios. These solutions are in GPE, and it turns out that the solution by 2D FEA for GPE from Figure 14b gives the same graph for  $K_{tz}$ . It is seen from Figure 14a that the 2D PE solution gives a much steeper function for  $K_{tz}$ , and it becomes possible to comprehend how wrong a solution that assumes infinite thickness is, when used for real structures.

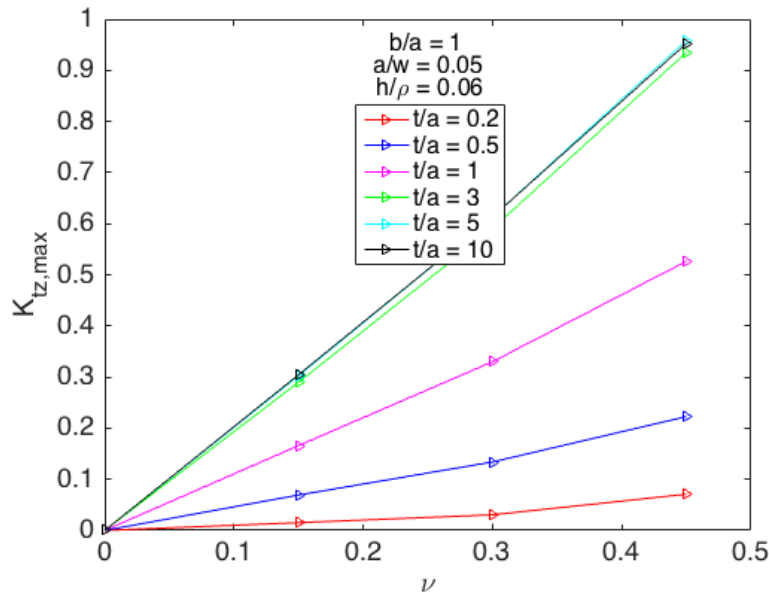
### 4.5.3 The effect of Poisson's ratio on the stress gradient

By studying the effect of thickness on the stress gradient it was found that the value at the free surface is higher than all other values inside the material. The other effect of thickness was that the lowest stress gradient was always placed at the point of maximum SCF. The effect of Poisson's ratio on the stress gradient is studied in Figure 35, to show how it affects both the value at the free surface of the structure and at the mid-plane. The reason why the point of maximum SCF was not considered, was simply because data from FEA at the mid-plane were already available and the stress gradients at the mid-plane are approximately equal to those at the point of maximum SCF, for all plate thicknesses studied.

When the Poisson's ratio goes from  $\nu = 0.1$  to  $\nu = 0.49$  for plates with large thickness, a large increase in the ratio of  $K_{t,max}/K_{t,surf}$  was found both by Yu et al. [8] and from FEA, as shown in Figure 33. Yu et al. found that this increase was simply due to a drastic reduction of the SCF at the free-surface with increasing Poisson's ratio. In Figure 35a the stress gradient at the free surface is studied, to



(a) Maximum SCF in  $z$ -direction when thickness is varied.



(b) Maximum SCF in  $z$ -direction when Poisson's ratio is varied.

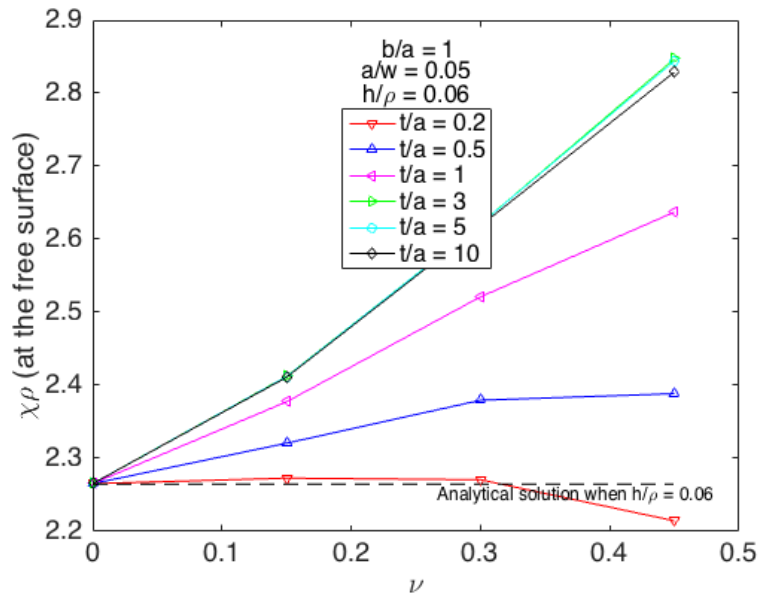
Figure 34: Maximum SCF in  $z$ -direction from FEA of 3D plates with central circular holes with varying thickness and Poisson's ratio.

see whether the decrease in SCF at the free surface affects the stress gradient. It is found from the figure that the stress gradient rather increases with increasing Poisson's ratio, and most rapidly for thick plates. This is an interesting development, where the stress decreases at the same time as the curve becomes steeper towards the notch root. It is however observed that the stress gradient decreases for the thinnest plate that was studied, and this curve is almost equal to the analytical solution for most Poisson's ratios.

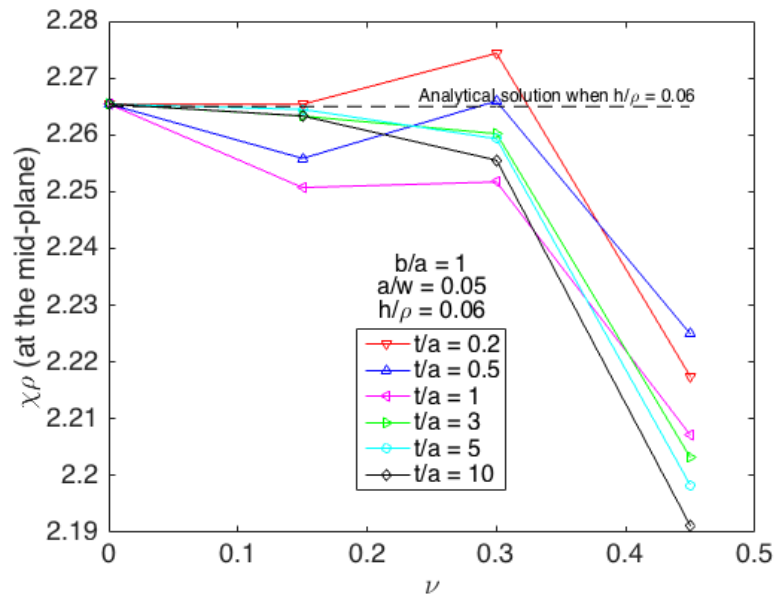
In Figure 35b the stress gradients found at the mid-plane for both thin and thick plates show a similar behaviour for small Poisson's ratios, which is close to the estimated theoretical solution for  $h/\rho = 0.06$ . However, the two thicknesses with highest maximum stresses ( $t/a = 0.5$  and  $1$ ) directly decrease when the Poisson's ratio goes from zero. The reason why the solution at  $\nu = 0$  is equal to the estimated theoretical solution for  $h/\rho = 0.06$  is similar to the one explained for  $K_{t,\max}$ . As there is only a longitudinal stress and strain acting when  $\nu = 0$ , the mesh remains unchanged in both  $x$ - and  $z$ -direction. For  $K_{t,\max}$  this meant that the value at  $h = 0$  was reached as the SCF result at the notch root became independent of the mesh. However, the stress gradient is still dependent on the mesh size, as it is calculated based on the results at the nodes and the distances between them. Because of this, the stress gradient approaches the estimated solution at  $h/\rho = 0.06$  rather than the solution at  $h = 0$ . From both Figure 35a and Figure 35b this is consistent.

Further, another observation from Figure 35b is that the stress gradient at the mid-plane, thus also at the point of maximum SCF, decreases with Poisson's ratio. The values found at  $\nu = 0.45$  are between 1.76% and 3.3% lower than the estimated theoretical solution. This confirms the trend found in Figure 31 for  $\nu = 0.3$ , and shows that the result is even more dramatic as Poisson's ratio increases further. There is a consistent decrease in stress gradient with increasing Poisson's ratio in Figure 35b for all plates apart from the two thinnest. The two thinnest plates show a more irregular behaviour before it properly decreases, and there are no valid assumptions as to why this happens apart from the actual effect of the Poisson's ratio. This result indicates that a full thickness evaluation would be interesting, where many more thicknesses are studied.





(a) Stress gradient at the plate free surface



(b) Stress gradient at the plate mid-plane

Figure 35: The stress gradient for varying Poisson's ratio at the a) free surface and b) mid-plane of the plate, as calculated from the FE-results.



## 5 Fatigue assessment based on 3D FEA

The FE-results have confirmed that the maximum stress is located inside, and never at the free surface, of the plate. This is the same as what has been found in other papers considering the 3D SCFs [7]–[9], [18]. Findings related to the 3D stress gradient however, has not yet been published by others. The FE-results showed that the maximum stress gradient was much higher than the analytical value, and located at the free surface of the plate. While the lowest stress gradient was always lower than the analytical value and located at the point of maximum stress. Some of the most critical factors for fatigue life is a high SCF and a low stress gradient [16], and the FE-results show that both these are found at the same point inside the plate. Thus, raising concerns about the true fatigue life of structures. A fatigue assessment is included in this thesis to show what the new findings mean for the fatigue life of structures, and will be compared to conventional methods based on analytical solutions and the FE-results at the free surface of the plate.

### 5.1 Formulae for fatigue

Depending on the method used for fatigue assessment, both the SCF and the stress gradient can be used in calculations. Here both the peak stress method, which only considers the maximum SCF, and the stress gradient method, which includes the stress gradient, are used to find the number of cycles to failure based on the FE-results. Some important factors that will not be considered, is that the probability of material defects increases with thickness (3D structure versus 2D) and the effective stress, as this remains a simple example to easily illustrate the potential weakness of conventional methods compared to the actual 3D behaviour of plates. In the following example, the results from a plate with thickness  $t/a = 3$  and an elliptic through-hole with  $b/a = 0.5$  is considered. The FEA was limited to linear elastic behaviour, and high-cycle fatigue will be considered where the mean-stress  $\sigma_m = 0$ .

#### 5.1.1 The peak stress method

With the peak stress method, calculations are based on the maximum stress amplitude at the notch root, found from

$$\sigma_{a,\max} = K_t S \quad (26)$$

where  $S$  is the applied stress at the gross section of the structure and  $K_t$  is the stress concentration factor at the notch root [20].

The number of cycles to failure can be found from the stress–life curve, the S–N curve, for the material. Assuming linear behaviour between  $\log S$  and  $\log N$ , the number of cycles to failure can be approximated by Basquin’s equation [22]:

$$\sigma_a = \sigma'_f(2N)^b \quad (27)$$

where  $\sigma'_f$  is the fatigue strength coefficient of the material,  $N$  is the number of cycles to failure and  $b$  is the fatigue strength exponent.

The maximum stress amplitude found in Eq.(26) can be inserted into Eq.(27) so that the number of cycles to failure can be calculated directly from the SCF and the applied stress, giving:

$$K_t S = \sigma'_f(2N)^b$$

and by rearranging the equation, the number of cycles to failure based on the peak stress method is:

$$N = \frac{1}{2} \left( \frac{K_t S}{\sigma'_f} \right)^{1/b} \quad (28)$$

### 5.1.2 The gradient method

The peak stress approach would only be accurate if the largest defect existed at the point of maximum stress. In reality, this is not likely. The gradient method is an approach to account for the whole region of highly stressed material [14]. The maximum stress amplitude as found in Eq.(26) is reduced by a support factor  $S_\chi$ , in the following manner:

$$\sigma_a = \frac{\sigma_{a,\max}}{S_\chi} = \frac{K_t S}{S_\chi}$$

where the support factor  $S_\chi$  depends on the relative stress gradient  $\chi$  and a material constant  $\rho_0$  at the notch root:

$$S_\chi = 1 + \sqrt{\rho_0 \chi}$$

As this is a "so called" corrected maximum stress amplitude, it can also be evaluated using Basquin’s equation, see Eq.(27). Thus, the gradient method is given by the following equation:

$$\frac{K_t S}{1 + \sqrt{\rho_0 \chi}} = \sigma'_f(2N)^b$$

where  $N$  is the number of cycles to failure.

By rearranging the equation, the number of cycles to failure based on the gradient method is:

$$N = \frac{1}{2} \left( \frac{K_t S}{(1 + \sqrt{\rho_0 \chi}) \sigma'_f} \right)^{1/b} \quad (29)$$

## 5.2 Fatigue constants

The material used for fatigue calculations is a SAE4340 quenched and tempered steel [22]. The material data is taken from the ASM Handbook [22] and the material constant  $\rho_0$  is found from a table provided in Pilkey [6]. All the relevant fatigue constants are presented in Table 5. In order for a direct relevance to the FEA results, the same applied stress  $S$  is used in the fatigue calculations. Apart from the fatigue constants, the same material constants as was used in 3D FEA applies, so that the Poisson's ratio  $\nu = 0.3$  and the Young's modulus  $E = 200$  GPa.

Table 5: Constants used for fatigue calculations.

S	$\sigma'_f$	$b$	$\rho_0$
100 MPa	1898 MPa	-0.09	50 $\mu\text{m}$

## 5.3 Fatigue life calculations

### 5.3.1 The peak stress method

The number of cycles to failure based on the peak stress method is found from Eq. (28), where the only variable is the SCF. The maximum SCF value found from FEA was higher than the analytical solution, while the SCF at the free surface of the plate was much lower than both the analytical solution and the maximum SCF from FEA. In Table 6 the fatigue life calculated from the peak stress method, using both the FEA results and the analytical solution, is presented.

Table 6: Comparing the fatigue life by the peak stress method, based on the analytical solution and the FEA results. Where both the FEA results at the point of maximum SCF and at the free surface are considered.

	$K_t S$	N
Analytical solution [1]	500 MPa	$1.37 \times 10^6$ cycles
Max SCF from FEA	520.8 MPa	$8.71 \times 10^5$ cycles
SCF at free surface from FEA	398.4 MPa	$1.71 \times 10^7$ cycles

The number of cycles to failure at the point of maximum SCF is by far the most critical. It is seen from Table 6 that the number of cycles to failure are all very large numbers. This indicates that  $S = 100$  MPa is close to the fatigue limit of the material [14]. The purpose of these results is however to illustrate the differences between the solutions, which is independent of the applied stress, and thus fully valid for applied stresses above the fatigue limit as well. This means that when changing the applied stress in Eq. (28), a lower number of cycles would be calculated, but the same differences between the solutions would be found.

Table 6 shows that when the analytical solution is used for calculating the fatigue life, it gives 1.573 times the lifetime found when actually considering the maximum SCF. This means that the fatigue life is overestimated by 57.3% when the analytical solution is used on plates with  $t/a = 3$ . An even larger overestimate is found when the SCF at the free surface is used for fatigue calculations, giving a fatigue life that is 19.6 times the fatigue life found at the point of maximum SCF.

### 5.3.2 The gradient method

The number of cycles to failure based on the gradient method is calculated from Eq. (29), where the fatigue life varies with both the SCF and the stress gradient. The stress gradient results from FEA were highest at the free surface and lowest at the point of maximum SCF. Table 7 gives the fatigue life found from the gradient method, based on the FEA results and the analytical solution. The «analytical» stress gradient used for these calculations is in fact the estimated theoretical value when  $h/\rho = 0.06$  ( $\chi\rho = 2.125$ ). This value is used so that the results become compatible, for a realistic comparison.

Table 7: Comparing the fatigue life by the gradient method, based on the analytical solution, and the FEA results at the point of maximum SCF and at the free surface.

	$K_t S$	$\chi$	N
Analytical solution [14]	500 MPa	1.7	$2.35 \times 10^7$ cycles
Max SCF from FEA	520.8 MPa	1.688	$1.49 \times 10^7$ cycles
SCF at free surface from FEA	398.4 MPa	1.976	$3.55 \times 10^8$ cycles

Table 7 shows that when considering the analytical solution for both the SCF and the stress gradient, the fatigue life becomes 1.577 times higher than when considering the values found at the point of max SCF. In other words, by considering the analytical solutions, the fatigue life might be overestimated by 57.7%, even after considering the effect of  $h/\rho$ . The result at the free surface of the structure is expected to deviate greatly from the other results, but is simply included to show why this approach should never be used. The results show that using the SCF

and stress gradient found at the free surface gives a fatigue life that is 23.8 times the fatigue life found at the point of maximum SCF.

Finding the maximum SCF from FEA is a relatively simple procedure, while finding the stress gradient is an extensive process, and based on this it is interesting to test whether the maximum SCF from FEA can be combined with the analytical stress gradient to give a realistic fatigue assessment. Here the analytical stress gradient found from literature should be applied, meaning  $\chi\rho = 11/5$ . Inserting the analytical relative stress gradient  $\chi = 1.76$  and  $K_{t,\max}S = 520.8$  into Eq. (29), the number of cycles to failure is found:

$$N = \frac{1}{2} \left( \frac{520.8}{(1.297)1898} \right)^{-1/0.09} = 1.57 \times 10^7 \text{ cycles}$$

which is 1.054 times higher than the result when both parameters are found from FEA at maximum SCF. By combining the maximum SCF found from FEA and the analytical stress gradient, a potential 5.4% overestimate of the actual lifetime could be expected.

## 5.4 Conclusion on fatigue life

Both the peak stress method and the gradient method show that the SCF and stress gradient should never be measured at the free surface for fatigue calculations. Both methods also show that a purely analytic approach is expected to overestimate the fatigue life by more than 50%. As the peak stress method is a conservative approach, the results using the analytical solution could probably be accepted. However, the gradient method is supposed to give a corrected view of the actual fatigue life and it shows that the fatigue life is actually greatly overestimated when using the analytical solutions.

The proposed approach, where the maximum SCF found from 3D FEA and the analytical stress gradient are combined, only results in a 5.4% error relative to the full 3D approach. Considering the amount of work required to perform a full 3D evaluation, this error is small and a good compromise. However, the full 3D approach where both the stress gradient and the maximum SCF from 3D FEA are used, is assumed to be the most accurate approach. In particular because it was found that the stress gradient decreases relative to the estimated theoretical approach with increasing Poisson's ratio. Even though the gradient found from 3D FEA can be replaced by the analytical solution, the results show that the 3D SCF is absolutely necessary in order to perform realistic fatigue calculations.

In the context of fatigue assessments of real structures, a lot of safety factors are involved. An overestimation of 5.4% quickly disappears when all safety factors are applied, and the proposed approach is hence both achievable and a reliable.





## 6 Discussion of method

In the preliminary study most of the choices of parameters and their effects on the results were presented. In this way, the thought process behind all of these choices were made visible. A thorough preliminary study was needed, as results with as high accuracy as possible was desired. For a large study, such as for this thesis, a preliminary study is believed to be crucial, as it provides the elementary understanding of FEM as well as the nature of SCFs.

A plate width with very low impact on the SCF was chosen in the preliminary study. The result of this is that the findings are specific to one plate-width. It was found most valuable to investigate the effect of thickness and Poisson's ratio, as the 3D effect of finite-width was already properly covered [9]. The idea behind choosing a value with low finite-width effect was that it would replicate the most general behaviour of wide plates. From this, the results presented should be reliable for all  $a/w \leq 0.05$  (from [9]). The  $a/w$  ratio that was chosen, was also already used in the three most relevant articles to this thesis [7]–[9].

Sources of errors that should be mentioned in regards to this thesis are based on the accuracy of FEM and the post processing of data from FEA. The FE-results should never be taken as accurate solutions, as it is a method meant for accurate approximations [13]. Intuitively it is assumed that the approximation is better, the more elements that are applied to the model [13], and the choice of mesh is carefully studied in the preliminary study to assure this. With reduced integration, it was shown that the maximum SCF for small plate thicknesses could be underestimated, but apart from this the overall accuracy was good. This means that the results are not expected to be much further from the real solution due to this choice. Nevertheless, reduced integration was the only possible option to solve the relevant structures with the desired accuracy.

The sources of errors in regards to the post processing of the FE-results are related to the methods used to collect stress data, and the approach used to calculate  $K_t$  and the stress gradient. These were all discussed in the preliminary study, and attempts to reduce the errors were made. As  $K_t$  is simply found from the stress value at the notch root node, it depends on the quality of the nodal stress. The stress gradient was calculated based on an approach introduced for a plate with a central circular hole. It was assumed that this method was accepted for all models, but the accuracy for other notches has not been tested. It should also be mentioned that in most of the figures presented, straight lines are used between the data points not as an attempt to assume what happens, but simply to make the figures easy to read. Straight lines are preferred over smooth lines, as straight lines clearly indicate that it is - by all means - just to connect the data points.

For 3D FEA, only central holes were studied. This was a conscious choice, due to computation time, as reducing the accuracy to achieve more was never

an option. The goal was always to do something reliable. A compromise was to include side-grooves in the 2D study, to present the difference in SCFs. The idea was that the difference could be considered to get an idea of the expected behaviour of the 3D results for side-grooves.

The results are in good correspondence with previous research, and the accuracy is similar, if not higher. As all relevant papers found on 3D SCFs are based on 3D FEA, any further advancements within this field relies on physical testing that can confirm these observations. Due to all the possible errors involved with FEA, and 3D FEA in particular, the final limiting factor is that there are no relevant physical evidence to compare with.

## 7 Conclusion

The effect of Poisson's ratio and thickness on the SCF and stress gradient was found from extensive 3D analyses of central holes and elliptical holes ( $b/a = 0.5$ ) in plates. A large range of thicknesses ( $t/a = 0.2, 0.5, 1, 3, 5, 10$ ) and Poisson's ratios ( $\nu = 0, 0.15, 0.3, 0.45$ ) were considered. The 3D model that was used for analyses, deviated 0.17% - 0.19% from the numerically estimated analytical solution for  $a/w = 0.05$ . Some characteristics that were already pointed out in previous research [7]–[9], was confirmed by the results. Some new details about the SCF behaviour was found, complemented by some very interesting findings about the 3D behaviour of the stress gradient. Complementing these results, a fatigue analysis was presented to show the importance of 3D FEA.

### 7.1 Key findings

1. The maximum SCF through the thickness remains at the mid-plane of the plate when  $t/a \leq 1.2$ . For all larger thicknesses studied, it was found that the maximum stress moves towards the free surface of the plate, but never reaches it. This complements the result by Vaz et al. [9] who showed that the maximum value remains at the mid-plane for  $t/a \leq 1.5$ .
2. For a central circular hole,  $K_{t,\max}$  is 21% higher than  $K_{t,\text{surf}}$  when  $\nu = 0.3$  and the difference increases to 40% when  $\nu = 0.45$ . For a central elliptic hole gave difference of 33% when  $\nu = 0.3$ . Confirming that the SCF measured at the free surface underestimates the stress state, as stated by She and Guo [7].
3. The highest stress gradient is always located at the free surface of plates, and for  $t/a \geq 3$  it is 12 - 14% higher than the theoretical solution.
4. The lowest stress gradient, which is most critical for fatigue, is always found at the point of  $K_{t,\max}$ , for all plate thicknesses and Poisson's ratios studied. The value is 1% lower than the theoretical solution when  $\nu = 0.3$  and decreases further with increasing Poisson's ratio. This result highlights the critical state of the material in this region, as a low gradient means that more material is highly stressed, increasing the probability of fatigue failure.
5. The peak value of  $K_{t,\max}$  increases by 9.65% from  $\nu = 0$  to  $\nu = 0.45$ . This is the same result as was shown by Yu et al.[8].
6. Fatigue analyses show that the value of  $K_{t,\max}$  is important for reliable results. The introduced approach, using the analytical stress gradient and  $K_{t,\max}$  from 3D FEA, gave a 5.4% overestimate of the fatigue life of a 3D structure, which is small compared to safety factors applied for fatigue.

## 7.2 Further work

It is suggested that further work within this field focuses on the following:

- Physical testing of 3D structures, which requires the development of appropriate methods to estimate the stress field inside the specimens.
- More elliptical shapes could be studied, in particular by changing  $b$ . It is interesting to look at more shapes where  $b < a$ , although this is thoroughly covered by She and Guo [7].
- The effect of Poisson's ratio on plates with elliptic through-holes with various radii of curvature. This requires powerful computers.
- The effect of  $a/w$  on the SCF, although this is studied by Vaz et al. [9].
- More thicknesses in the range of  $0 \leq t \leq 3$ , where the effect of thickness on SCF is largest. Larger thicknesses are not interesting, as a clear sign of GPE is found for  $t=10a$  for all models studied.
- A study of plates with central spheroids would complement the findings of this thesis very well.

## Bibliography

- [1] C. Inglis, ‘Stresses in a plate due to the presence of cracks and sharp corners’, *Transactions of the Institute of Naval Architects*, vol. 55, pp. 219–241, 1913.
- [2] S. Timoshenko and J. Goodier, *Theory of Elasticity*, 3rd ed. New York: McGraw-Hill, 1970.
- [3] H. Neuber, *Theory of Notch Stresses: Principles for exact stress calculation*. Michigan: J. W. Edwards, 1946.
- [4] J. R. Barber, *Elasticity - Solid Mechanics and Its Applications*, 3rd ed. Netherlands: Springer Science Business Media, 2010, p. 534.
- [5] R. Roark, *Roark’s formulas for Stress and Strain*, 7th ed. New York: McGraw-Hill, 2001.
- [6] W. D. Pilkey, *Peterson’s Stress Concentration Factors*, 2nd ed. Hoboken, New Jersey: John Wiley & Sons, 1997.
- [7] C. She and W. Guo, ‘Three-dimensional stress concentrations at elliptic holes in elastic isotropic plates subjected to tensile stress’, *International Journal of Fatigue*, vol. 29, no. 2, pp. 330–335, 2007.
- [8] P. Yu, W. Guo, C. She and J. Zhao, ‘The influence of poisson’s ratio on thickness-dependent stress concentration at elliptic holes in elastic plates’, *International Journal of Fatigue*, vol. 30, no. 1, pp. 165–171, 2008.
- [9] M. Vaz, J. Cyrino and G. Silva, ‘Three-dimensional stress concentration factor in finite width plates with a circular hole’, *World Journal of Mechanics*, vol. 03, no. 03, pp. 153–159, 2013.
- [10] D. Bellett, D. Taylor, S. Marco, E. Mazzeo, J. Guillois and T. Pircher, ‘The fatigue behaviour of three-dimensional stress concentrations’, *International Journal of Fatigue*, vol. 27, no. 3, pp. 207–221, 2005.
- [11] E. Siebel and M. Stieler, ‘Non-uniform stress distribution in the case of fatigue stresses’, *Z. VER. DTSC. ING.*, vol. 97, no. 5, pp. 121–126, 1955.
- [12] M. Filippini, ‘Stress gradient calculations at notches’, *International Journal of Fatigue*, vol. 22, no. 5, pp. 397–409, 2000.
- [13] K. Bell, *An engineering approach to Finite Element Analysis of linear structural mechanics problems*. Trondheim, Norway: Akademika forlag, 2013.
- [14] J. Schijve, ‘Stress gradients around notches’, *Fatigue and Fracture of Engineering Materials and Structures*, vol. 3, no. 4, pp. 325–338, 1980.
- [15] J. Fish and T. Belytschko, *A First Course in Finite Elements*. Chichester, England: John Wiley and Sons, 2007.

- [16] J. Schijve, *Fatigue of Structures and Materials*, 2nd ed. Netherlands: Springer Science Business Media, 2009.
- [17] Dessault-Systèmes, *ABAQUS/Standard Analysis User's Manual*. Providence, Rhode Island: Dessault-Systèmes Simulia Corp., 2014.
- [18] Z. Yang, C. Kim, C. Cho and H. Beom, 'The concentration of stress and strain in finite thickness elastic plate containing a circular hole', *International Journal of Solids and Structures*, vol. 45, no. 3-4, pp. 713–731, 2008.
- [19] T. Megson, *Aircraft Structures for Engineering Students*, 4th ed. Oxford, England: Butterworth-Heinemann, 2007.
- [20] N. E. Dowling, *Mechanical Behaviour of Materials - Engineering methods for deformation, fracture and fatigue*, 4th ed. Boston, Massachusetts: Pearson, 2013.
- [21] T. Anderson, *Fracture Mechanics - Fundamentals and Applications*, 3rd ed. Boca Ranton, Florida: Taylor & Francis, 2005.
- [22] B. Boardman, 'Fatigue resistance of steels', *ASM Handbook, Volume 1: Properties and Selection: Iron, Steels, and High-Performance Alloys*, pp. 673–688, 1990.

## A Appendix: The finite element models

### A.1 Input parameters for the FE-model

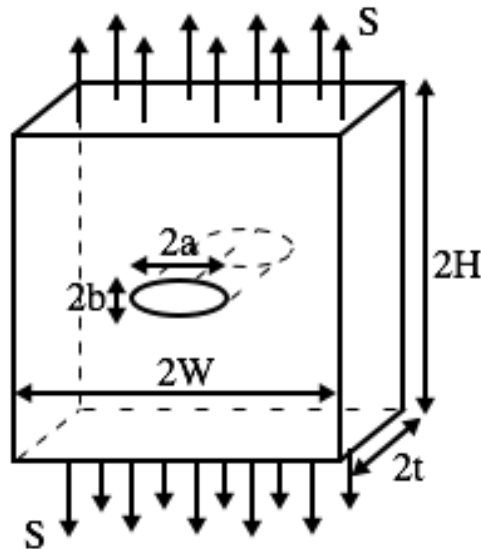
All FEAs, both in 2D and 3D, were modelled with the same parameters. The material constants and geometrical parameters used for FEA were:

Applied stress	$S$	100 MPa
Half-width of plate	$w$	100 mm
Half-height of plate	$h$	100 mm
Half-thickness of plate	$t$	1 mm – 50 mm
Major radius of ellipse	$a$	5 mm
Minor radius of ellipse	$b$	0.5 mm, 1 mm, 2 mm
Young's modulus	$E$	200 GPa
Poisson's ratio	$\nu$	0, 0.15, 0.3, 0.45

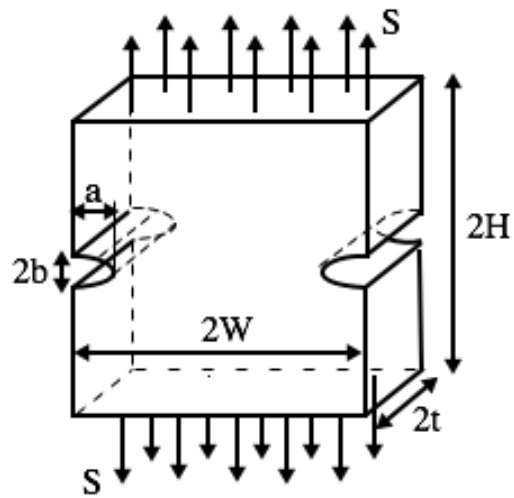
### A.2 The 3D structures studied

The different structures that were studied, with their respective geometrical properties, are presented below:

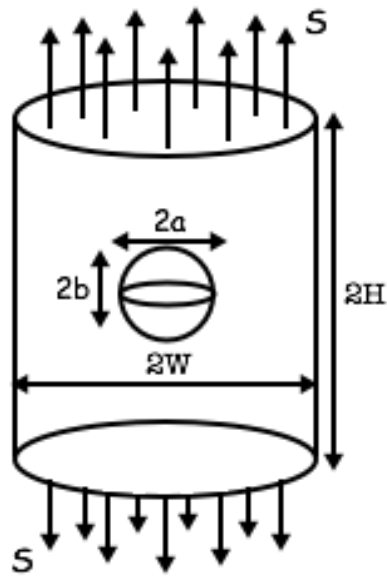
#### 1) Plate with central elliptic through-hole:



2) Plate with side-grooves:

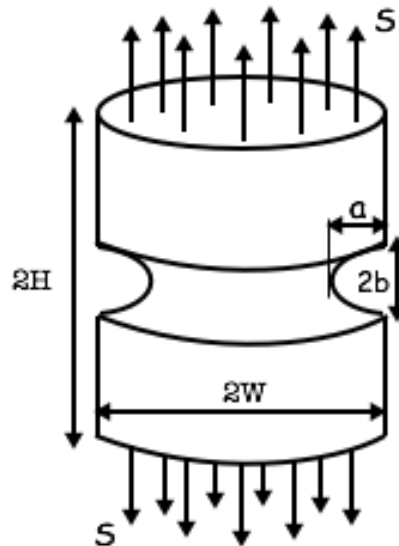


3) Cylinder with central sphere/spheroid:





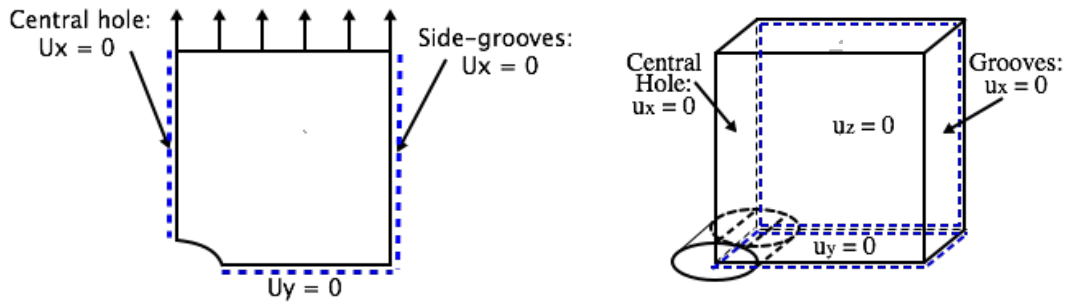
#### 4) Cylinder with circumferential grooves:



### A.3 Boundary conditions for FEA

As the FE-software does not require modelling of the full structures, the symmetry planes found in the structures above can be applied as boundary conditions to simplify the models.

**Boundary conditions for plates:** In 2D, only 1/4 of the model needs to be considered after applying two boundary conditions. In 3D, only 1/8 of the model needs to be considered after applying an additional boundary condition through the half-thickness of the plate. The figures below shows the models that were used, with the boundary conditions for both central holes and side-grooves in plates. The parameter  $U$  is used for displacement, and the subscript explains in what direction the displacement is restricted.



**Boundary conditions for cylinders:** The whole 3D behaviour of cylinders can be captured from a 2D model when an axisymmetric line is added as a boundary condition. The figures below shows the models needed and the boundary conditions for both cylinders with circumferential grooves and cylinders with central spheres. In these figures the displacement is labelled  $U_{22}$  to avoid confusion, as the coordinate system for cylinders is different than for plates. The subscript refers to displacement in the longitudinal direction. The left figure is for a central sphere and the right figure is for circumferential grooves.

